

Spatial specificity of the enhanced dip inherently induced by prolonged oxygen consumption in cat visual cortex: Implication for columnar resolution functional MRI

Mitsuhiro Fukuda,^a Ping Wang,^a Chan-Hong Moon,^a Manabu Tanifuji,^b and Seong-Gi Kim^{a,*}

^aBrain Imaging Research Center, Department of Neurobiology, University of Pittsburgh, 3025 East Carson Street, Pittsburgh, PA 15203, USA

^bLaboratory for Integrative Neural Systems, Brain Science Institute, The Institute of Physical and Chemical Research (RIKEN), 2-1 Hirosawa, Wako-shi, Saitama 351-0198, Japan

Received 22 December 2004; revised 13 July 2005; accepted 15 September 2005
Available online 27 October 2005

Since changes in oxygen consumption induced by active neurons are specific to cortical columns, the small and transient “dip” of deoxyhemoglobin signal, which indicates an increase in oxygen consumption, has been of great interest. In this study, we succeeded in enhancing and sustaining the dip in the deoxyhemoglobin-weighted 620-nm intrinsic optical imaging signals from a 10-s orientation-selective stimulation in cat visual cortex by reducing arterial blood pressure with sodium nitroprusside (a vasodilator) to mitigate the contribution of stimulus-induced blood supply. During this condition, intact spiking activity and a significant reduction of stimulus-induced blood volume changes (570-nm intrinsic signals) were confirmed. The deoxyhemoglobin signal from the prolonged dip was highly localized to iso-orientation domains only during the initial ~2 s; the signal specificity weakened over time although the domains were still resolvable after 2 s. The most plausible explanation for this time-dependent spatial specificity is that deoxyhemoglobin induced by oxygen consumption drains from active sites, where spiking activity occurs, to spatially non-specific downstream vessels over time. Our results suggest that the draining effect of pial and intracortical veins in dHb-based imaging techniques, such as blood oxygenation-level dependent (BOLD) functional MRI, is intrinsically unavoidable and reduces its spatial specificity of dHb signal regardless of whether the stimulus-induced blood supply is spatially specific.

© 2005 Elsevier Inc. All rights reserved.

Keywords: BOLD; Brain mapping; CBF; CBV; Hemodynamic response; Hypotension; Sodium nitroprusside; Intrinsic signal; Optical imaging; Ocular dominance column; Orientation column

Introduction

Non-invasive mapping of functional cortical columns with common neural properties is critical to understanding how the brain works. Since neural activity induces a focal increase in glucose and oxygen consumption rates, the metabolic response is supposed to be localized to the active site (Lowel et al., 1987; Thompson et al., 2003; Woolsey et al., 1996). Therefore, focal increases of deoxyhemoglobin (dHb) produced by the oxygen consumption change may precisely indicate the location of neural active sites. This expectation was confirmed with intrinsic optical imaging spectroscopy studies (Malonek and Grinvald, 1996), which showed that the early increase of dHb signal (referred to as the “dip”, i.e., metabolic response) is better localized to orientation-selective columns in the cat visual cortex than the late decrease of dHb signal due to an over-compensation of cerebral blood flow (CBF). Similarly, cortical columns in the cat visual cortex were successfully mapped only by the early dip in blood oxygenation level-dependent functional magnetic resonance imaging (BOLD fMRI (Ogawa et al., 1990)) but not by late responses at high magnetic fields (Kim et al., 2000a). Thus, the early dip has been of great interest to the functional imaging community (Hennig et al., 1994; Hu et al., 1997; Menon et al., 1995).

However, due to the small and transient nature of the early negative BOLD dip (Buxton, 2001; Duong et al., 2000a; Jezzard et al., 1997; Kim et al., 2000b; Logothetis, 2000) and consequently the low signal-to-noise ratio (SNR), it is difficult to routinely map sub-millimeter-scale functional columns from this dip. Alternatively, brain activity has been commonly mapped from the positive BOLD signal, which indicates a decrease in dHb (i.e., an over-compensated hemodynamic response), although the spatial specificity of this signal is poor compared to metabolic response. The poor spatial specificity of the *late* dHb responses (positive BOLD) can be explained by two hypotheses: (I) widespread CBF and cerebral blood volume (CBV) responses beyond the site of spiking

* Corresponding author. Fax: +1 412 383 6799.

E-mail address: kimgsg@pitt.edu (S.-G. Kim).

Available online on ScienceDirect (www.sciencedirect.com).

activity (Malonek and Grinvald, 1996) and (II) draining of dHb from the active site to non-specific downstream vessels (Duong et al., 2000a). Under normal physiological conditions, the increased oxyhemoglobin supply (i.e., CBF increase) and dHb drain occur simultaneously, making separation non-trivial. In order to decouple these two hypotheses, we propose to modulate the CBF and CBV responses induced by neural activity but without changing neural activity and oxygen consumption rates.

In this paper, the spatial specificity of dHb signals to iso-orientation columns is investigated in the absence of evoked CBF and CBV responses (i.e., conditions matching those of the early dip); these studies were performed in cat visual cortex by using optical imaging of intrinsic signals (OIS), which measures changes in light reflection from the cortical surface (Blasdel and Salama, 1986; Grinvald et al., 1986) accompanied by hemodynamic response to neural activity. To this end, dHb-weighted 620-nm OIS and CBV-weighted 570-nm OIS (for review, see Bonhoeffer and Grinvald, 1996) evoked by orientation-selective gratings were measured at normal and low blood pressure (BP) induced by sodium nitroprusside (sNP). Since blood vessels are considerably dilated at low BP (Endrich et al., 1987; Kontos et al., 1978), any further increase in CBF and CBV due to visual stimulation (i.e., 570-nm OIS) will be significantly reduced. Thus, spatiotemporal dynamics of 620-nm OIS inherently induced by oxygen consumption change can be measured. If, during stimulation at low BP, the 620-nm OIS is not localized to active sites, then the spatial localization of the dHb signal is unlikely due to non-specific blood supply but rather due to the draining of dHb. This investigation will determine the intrinsic spatial specificity of dHb-based functional imaging techniques such as conventional BOLD fMRI and OIS. The companion work studied with fMRI under similar low BP conditions is reported elsewhere (Nagaoka et al., in press).

Materials and methods

Ten cats (1.3–2.0 kg, 11–19 weeks) were used in this study (8 cats for optical imaging and 2 cats for multiple-unit recording). All experimental procedures were approved by the Institutional Animal Care and Use Committee at the University of Pittsburgh.

Animal preparations and physiological conditions

Each cat was initially treated with atropine sulfate (0.05 mg/kg, sub-cutaneous injection) and anesthetized with a sub-cutaneous injection of a mixture of ketamine (20 mg/kg) and xylazine (1 mg/kg). The cat was then intubated and mechanically ventilated (1–2% isoflurane in a mixture of initially 50% N₂O and 50% O₂, and subsequently 70% N₂O and 30% O₂). The femoral artery and vein were cannulated for monitoring arterial blood pressure and injection of drugs, respectively. An intravenous catheter was also inserted into the cephalic vein for continuous infusion of pancuronium bromide (0.2 mg·kg⁻¹·h⁻¹) mixed in 5% dextrose Ringer's solution by an infusion pump (Product No. 55-3333, Harvard Apparatus, MA). The cat was then placed in a stereotaxic apparatus (SN-3N, Narishige, Japan). Electroencephalogram (EEG) electrodes were implanted in the frontal bone, and a metal head post and a recording chamber (a 17.5-mm inner diameter) were mounted on the skull with dental acrylic cement. The

chamber was placed so that it included A10-P5 and L0-L5 in Horsley–Clarke coordinate; this region roughly corresponds to the location of area 18 in the lower quadrant of the visual field, which is approximately between the vertical meridian and ~25° into the contralateral field, and between the horizontal meridian and ~25° into the lower field (Tusa et al., 1979). After performing a craniotomy inside the chamber, the dura mater was resected. The inside of the chamber was then filled with ~1.5% agarose (Product No. 05065, Fluka BioChemika, Switzerland) and sealed with a round glass cover slip. After surgery, the stereotaxic frame was removed, and the cat was secured by the head post under a microscope objective for optical imaging. Recordings commenced 1–2 h after the surgery.

To assess the anesthetic level of the cats throughout surgery and experiments, we continuously monitored their rectal temperature, EEG, electrocardiogram, arterial blood pressure, arterial oxygen saturation (SpO₂) and expired-CO₂. These parameters were recorded with BIOPAC (MP150, BIOPAC Systems Inc., CA) for later analyses. Rectal temperature was maintained between 38.1 and 38.7°C with a feedback regulated heating pad system (FHC, Inc., ME). Expired-CO₂ was monitored by capnometer (Capnomac Ultima, Datex Omeda, Finland) and maintained in the range of 3.1–3.9% by adjusting the volume or rate of the ventilator (RSP-1002, Kent Scientific, CT) or both. SpO₂ measured with a pulse oximeter (8600 V, NONIN Medical, Inc., Denmark) was almost 100%. Arterial blood gas analysis (Stat profile pHox, Nova Biomedical, MA) was performed under normal blood pressure conditions for nine cats (these measurements were not performed for one of the cats used for multiple-unit recording) as follows (mean ± one standard deviation (SD)): P_{CO2} (24.3 ± 1.9 mm Hg, *n* = 9), P_{O2} (204.9 ± 19.1 mm Hg, *n* = 8 (the measurement could not be performed for one of the cats used for optical imaging)), and pH (7.46 ± 0.03, *n* = 9). The isoflurane concentration in a gas mixture of 70% N₂O and 30% O₂ was maintained at the same level during each set of recording for individual cats (usually 0.85–1.0%), which consisted of control (before vasodilator injection), low BP (during injection), and recovery (post-injection) conditions. The range of mean arterial blood pressure (MABP) for control was 76.1–100.9 mm Hg, and that for recovery was 81.6–105.1 mm Hg. These were within the normal range of MABP for cats under ~1% isoflurane anesthesia (Harel et al., 2002a; Zhao et al., 2004a). The range of MABP for low BP was 40.1–55.4 mm Hg.

Sodium nitroprusside-induced low blood pressure

To reduce arterial BP, a vasodilator (sodium nitroprusside dehydrate (sNP), Abbott Laboratories, IL) was injected intravenously for ~25 min (total amount of injection: 0.32–0.59 mg/kg). The sNP (2.5, 5.0 or 7.5 mg) was dissolved in 6 ml of either saline or a mixture of saline and Dextran 40 or 70 (Baxter, IL). The vasodilator infusion rate was dynamically adjusted (between 0.0003 ml/min (initial) and max. 0.08 ml/min to avoid cyanide toxicity) by manually controlling an infusion pump (PHD2000, Harvard Apparatus) to maintain MABP at ~45 mm Hg for ~25 min during optical imaging and for ~15 min during multiple-unit recording. The initial drop in MABP tended to reach ~40 mm Hg, and in two cases, EEG signals became flat at that period. After termination of the vasodilator injection, MABP returned to levels similar to control values (before the vasodilator injection) within ~5 min.

Visual stimuli

All visual stimuli were presented binocularly. Square-wave high-contrast gratings were generated by a graphic video board (VSG2/5, Cambridge Research Systems, United Kingdom) controlled by a custom software written in MATLAB 6.5 (MathWorks, Inc., MA) or Microsoft Visual C++ 6.0 and were presented on a 21-in. CRT monitor (800 × 600 pixels and 100 Hz refresh rate, GDM-F520, Sony). The spatial and temporal frequencies of the gratings were 0.15 cycle (c) per degree and 2 c/second (s) respectively for selective stimulus of area 18 (Bonhoeffer et al., 1995; Issa et al., 2000). The direction of the motion of the gratings was reversed every 0.5 s during visual stimulation. The cat's pupils were dilated with ophthalmic solutions of atropine (1%), phenylephrine hydrochloride (2.5%), and proparacaine hydrochloride (0.5%). Contact lenses (± 0.0 D, Danker Laboratories Inc., FL) were fitted to the eyes to prevent corneal drying. The visual field center was roughly estimated by projecting images of optic disks and retinal vessels onto the CRT monitor (Bishop et al., 1962) whose distance was then placed where the best focus of the optic disks and the retinal vessels were obtained (19–31 cm from eyes; visual field 70°–115° wide and 54°–88° high).

Optical imaging

The intrinsic signals were recorded with a custom-made imaging system consisting of tandem lens optics (Ratzlaff and Grinvald, 1991) (i.e., face-to-face combination of a projection lens (50 mm F/1.2, Nikon, Japan) and an objective lens (50 mm F/1.2, Nikon)), a charge-coupled device (CCD) camera (CS8310, 640 × 480 pixels, Tokyo Electric Industry, Japan) and a 10-bit frame grabber board (either Pulsar or Corona-II, Matrox Graphic Inc., Canada). The imaging area was 8.8 × 6.6 mm². For seven of the eight cats, the camera was focused on the cortical surface to detect vascular responses on pial vessels. The diaphragm of the projection lens was set to F/2.8 for a large depth of field. For the remaining one cat, the camera was refocused 500 μ m below the cortical surface, and the diaphragm of the projection lens was set to F/1.2 for a shallow depth of field as with conventional optical imaging. Since the results obtained from both depth of field were essentially the same, both data were pooled together for analyses. Images were captured at 1/30 s with the frame grabber board controlled by

custom software written in Microsoft Visual C++ 6.0. To improve SNR and also reduce data size, temporal averaging of 15 consecutive images and spatial binning of 2 × 2 pixels were performed before saving the acquired images. Thus, the final temporal and spatial resolutions of the saved images were 0.5 s/image and 27.5 × 27.5 μ m²/pixel, respectively. The cortical surface was illuminated through an interference filter (540, 570, or 620 ± 10 nm, Oriel Instruments, CT) using a bifurcated fiber optic bundle (SP77533, Oriel Instruments, CT) that was connected to a tungsten–halogen light source (Model No. 66881 and 68931, Oriel Instruments, CT).

Experimental design

Experimental protocol was outlined in Table 1. In all studies, cortical surface imaging with 540-nm wavelength and four-orientation 620-nm OIS were performed. Additionally, single-orientation 620-nm and/or 570-nm OIS were measured from the same cortical surface, or multiple neural recordings were performed as follows.

Cortical surface imaging with 540 nm

Initially, an image of pial vascular pattern was taken with 540-nm wavelength, at which light absorption by hemoglobin is largest.

Four-orientation 620-nm OIS

After acquiring an image of surface vascular patterns, iso-orientation domains for a particular orientation were mapped with 620-nm OIS, which is empirically known to give excellent contrast. To obtain the iso-orientation map efficiently and quickly with the conventional cocktail blank method (described in OIS data analysis), four orientations (0°, 45°, 90°, and 135°) were used with short stimulus duration (2 s) and inter-stimulus interval (2 s). Each stimulation run consisted of 1-s of pre-stimulus homogenous gray (i.e., 2 images) and 2-s stimulus with a moving grating presented at one of the four orientations followed by 1-s of post-stimulus homogenous gray. Twenty runs were repeated for each orientation stimulus (i.e., total recording time, ~2.7 min). The four orientations were presented at a sequential order (from 0° to 45°, 90° and 135°). Based on our experience, the orientation presentation order (e.g., random or sequential presentation) does not affect iso-orientation maps in this short time recording.

Table 1
Experimental design

Experiment	Purpose	MABP	Stimulation	Remarks
Cortical surface imaging with 540 nm	Visualization of vessels	Normal	None	– Separation of tissue and vessel ROIs
Four-orientation 620-nm OIS	Mapping iso-orientation domains	Normal	4 orientations, 2-s stimulation duration 2-s inter-stimulus interval (ISI)	– “Reference” for single-condition iso-orientation maps – Assignment of active and inactive domains for quantitative analyses
Single-orientation 570-nm OIS	Spatiotemporal dynamics of CBV responses	Normal and Low	One orientation, 10-s stimulation 64-s ISI (49 s in one case)	– Determination of whether functional CBV response is decreased at low BP
Single-orientation 620-nm OIS	Spatiotemporal dynamics of dHb responses	Normal and Low	One orientation, 10-s stimulation 64-s ISI	– Enhancement of the dip at low BP – Spatial specificity of the prolonged dip
Multiple-unit recording	Fidelity of neural activity	Normal and Low	4 orientations 10-s stimulation 5-s ISI	– Selectivity of neural activity during low BP

Single-orientation 570- and 620-nm OIS

To determine contribution of CBV response or spatial specificity of dHb signal, 570-nm or 620-nm OIS induced by 10-s visual stimulation were recorded during normal and low BP conditions respectively ($n = 5$ cats for each wavelength, 2 of them for both wavelengths). The 10-s stimulation duration is relevant to typical block-design fMRI studies. To achieve efficient signal averaging in a limited experimental time during the low BP, only single orientation (0° , 45° , 90° , or 135°) was presented. Twenty single-orientation stimulation runs were continuously acquired at each of normal BP, low BP, and recovery sessions; each run consisted of 10 s of pre-stimulus stationary grating and a 10-s moving grating followed by 54 s (39 s for one 570-nm OIS) of post-stimulus stationary grating to allow the signals to return to pre-stimulus baseline (i.e., inter-stimulus interval was 64 or 49 s). Since results obtained from the two stationary grating periods (64 and 49 s) were essentially the same, both data were pooled together for analyses. For low BP sessions, OIS recordings were started after the MABP reached a desired level (~ 45 mm Hg). One hour after termination of vasodilator injections, the recovery of the signals was confirmed.

Multiple-unit recording

Spiking activity of multiple neurons was recorded extracellularly from single tungsten microelectrodes (Catalog #UEWLFFL-MNN1E, Frederick Haer and Co. Brunswick, ME) during control (normal BP), low BP, and recovery conditions. The electrode was inserted using a hydraulic microdrive (Narishige MO-81, Japan) into an iso-orientation domain pre-determined with the *Four-orientation 620-nm OIS* recording. The spikes whose amplitudes exceeded a certain threshold, which was set near background activity, were detected at 40 kHz using a spike acquisition system (Plexon Inc, Dallas, Texas). Stimulus consisted of a 2-s homogeneous gray and a 10-s duration moving grating with one of four orientations (0° , 45° , 90° , and 135°) followed by 3-s homogenous gray. For each orientation stimulus, five runs were averaged and spike firing rates in 100-ms bins during stimulation were calculated to determine the selectivity of multiple neurons recorded.

OIS data analysis

All data were analyzed with MATLAB 6.5. After averaging across stimulation runs for each experiment, three sorts of maps (*single-condition raw activity*, *differential iso-orientation*, and *single-condition iso-orientation* maps) were generated as described in detail below. All the values below are reported as mean \pm 1 SD. Statistical significance was examined by ANOVA and two-tailed paired t test. P values of less than 0.05 were considered to be statistically significant.

Averaging across stimulation runs

To increase SNR, OIS runs were averaged. For the experiment of *Four-orientation 620-nm OIS*, all 20 OIS runs (4 s/each run; 1-s pre-stimulus and 3-s post-stimulus onset) were averaged for each orientation. For the experiment of *Single-orientation 570 and 620-nm OIS*, OIS runs were first chopped into a period of 40 s (10-s pre-stimulus and 30-s post-stimulus onset) and screened based on MABP during each 40-s run before averaging. To obtain the MABP during each run, MABP at every cardiac cycle was calculated from the sum of two-thirds of diastolic BP and one-third of systolic BP, and all the MABP for 40 s were averaged. Then one

SD of the mean for MABPs across 20 runs (15 runs for low BP sessions, the first five runs were excluded from analyses because the reflected light intensity was not yet stable (see Fig. 2B right panel)) was calculated. Finally, OIS runs whose MABP were within a range of the one SD were averaged. At each BP condition, one averaged run was determined.

Generating single-condition raw activity maps

Then the first frame analysis (for review, see Bonhoeffer and Grinvald, 1996) was performed on the averaged run to reduce the contribution of slow signal fluctuations related with vasomotion (e.g., ~ 0.1 Hz (Mayhew et al., 1996)) to OIS time courses; the average of two images (i.e., 1 s) just before stimulus onset (pre-stimulus image, R) was subtracted from all images ($R(t)$, t is time from the stimulus onset). The subtraction images ($\Delta R = R(t) - R$) were then divided by the pre-stimulus image (R), so that the pixel values indicate a relative change of reflectance ($\Delta R/R$; 0, no change of light reflection; $-$ (negative sign), decrease of light reflection (i.e., increase of light absorption); $+$ (positive sign), increase of light reflection (i.e., decrease of light absorption)). This first frame analysis was applied to both the *Four-orientation 620-nm OIS* and *Single-orientation 570 and 620-nm OIS* experiments; it is equivalent to a percentage signal change induced by stimulation, which is commonly used in functional MRI. The image generated by the first frame analysis is referred to as a “single-condition raw activity map” (Fig. 1B). All images in the Results section are shown as gray-scale code, where brightness of gray shows intensity of light reflection from pre-stimulus baseline (i.e., darkening and lightening represent decrease and increase in light reflection, respectively).

Generating differential iso-orientation maps

As seen in the single-condition raw activity map (Fig. 1B) or in the map profile (Fig. 1C), OIS is induced not only in the domain specific to a particular orientation but also in all other domains for other orientations, resulting in orientation-specific and -non-specific components (see also Frostig et al., 1990; Grinvald et al., 1986; Malonek and Grinvald, 1996). To remove the orientation-non-specific component and to quantitatively determine iso-orientation domains specific to a particular orientation, we used the cocktail blank data analysis method, which is commonly used to generate iso-orientation maps (for review, see Bonhoeffer and Grinvald, 1996). To this end, first, single-condition raw activity maps for the four orientations (0° , 45° , 90° , and 135°) were obtained from the experiment of *Four-orientation 620-nm OIS* (i.e., 4-s recording for each orientation). Each map was averaged from 0.5 to 3 s after the stimulus onset (the image at 0 s was not included in the average because the signal did not emerge clearly) to increase SNR. Then the resulting four single-condition raw activity maps were averaged to generate a cocktail blank image. Finally, the cocktail blank image was subtracted from the raw activity map with one of the four orientations, and the spatial filter (Fig. 1D) was applied (see below). We will refer to the generated map as a “differential iso-orientation map” (Fig. 1F). This map was used to quantitatively determine iso-orientation domains (see ROI analysis).

Generating single-condition iso-orientation maps

The local modulations specific to a particular orientation (orientation-specific component) can also be extracted from global modulations, which are independent of stimulus orientation

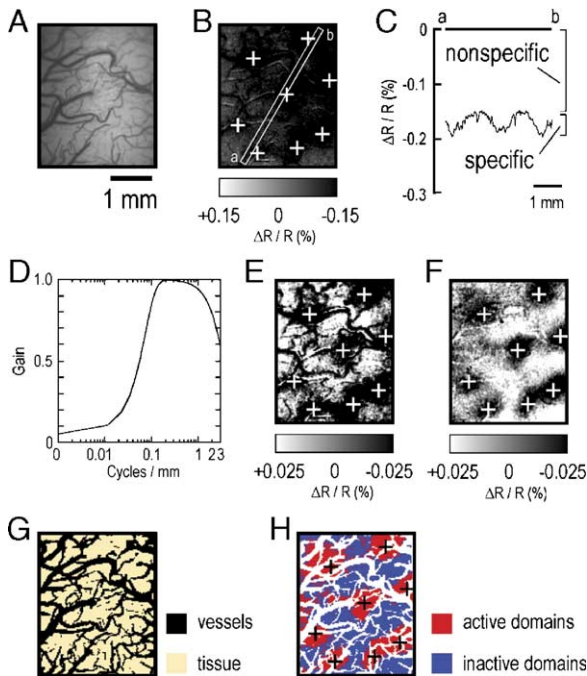


Fig. 1. Cortical activation map generation for analysis of OIS data. (A) A cortical surface image (540 nm) showing vessels for correlation with the maps (620 nm) in panels B, E, F, G, and H. (B) A single-condition raw activity map. The map was obtained by averaging relative change of reflectance images after stimulus onset (0.5–10 s, the image at 0 s was not included in the average because the signal did not emerge clearly). Global absorption increase was observed as a darkening of the entire region (grating at 45° orientation). (C) The profile along the line a-b in map B. (D) Properties of the spatial filter used to remove the global absorption change. (E) A single-condition iso-orientation map. The global absorption change was filtered from the single-condition activity map in panel B. Black patches are now responses specific to the grating at 45° orientation. (F) A differential iso-orientation map. Locations of black patches were determined on this map and marked with white crosses on all maps. (G) Separation of pial vessels (black) and tissue (yellow) based in image A. (H) Separation of active (red) and inactive (blue) domains. Based on the differential iso-orientation map F, the ROI was sub-divided into active and inactive domains for the grating at 45° orientation. Maps were demonstrated with normal BP data (average for 12 runs). See Materials and methods for processing details.

(orientation-non-specific component), by simply applying a spatial filter (Fig. 1D) to the single-condition raw activity map. We will refer to this spatial filtered map as a “single-condition iso-orientation map” (Fig. 1E). The map was obtained from the experiment of *Single-orientation 570- and 620-nm OIS*. This map was used to demonstrate whether iso-orientation domains determined by single-orientation are consistent with those determined by four-orientation stimuli (Figs. 6 and 9). Properties of the filter were determined by the difference of two Gaussian functions ($f(x) = e^{-\frac{x^2}{2\sigma_1^2}} - e^{-\frac{x^2}{2\sigma_2^2}}$, where $\sigma_1 = 0.4$ for low pass frequency, $\sigma_2 = 0.008$ for high pass frequency). The spatial domain image (Fig. 1B) was first transformed into a frequency domain image and then multiplied by the spatial filter (Fig. 1D) to remove low and high frequency components. Finally, the filtered frequency image was inversely transformed into the spatial domain image (Fig. 1E). Black patches in this map represent preferential activation by a particular stimulus orientation.

ROI analysis

To determine spatiotemporal responses induced by a stimulus with a single-orientation, “tissue” and “vessel” regions were chosen (Fig. 1G); the separation between tissue and vessel regions was determined on the cortical surface image taken at 540 nm (see Fig. 1A). Since vessels absorb more light than tissue at this wavelength, vessels appear dark in cortical surface images at 540 nm. Pixels containing signal from pial vessels (a pixel size was $27.5 \times 27.5 \mu\text{m}^2$) were assigned to the vessel region of interest (ROI), and the remaining pixels were the tissue ROI (Fig. 1G). The ratio of vessel ROI to tissue ROI was 0.67 ± 0.06 ($n = 7$ cats). In one cat, due to blurring of pial vessels caused by defocusing camera from cortical surface, the vessel ROI was larger than tissue ROI (the ratio was 1.96), however, this does not affect the result. Tissue ROI was further sub-divided into “active” and “inactive” domains based on the differential iso-orientation map. The pixels having negative values ($-\Delta R/R\%$) in the differential iso-orientation map (Fig. 1F) were assigned to active domains, and the remaining pixels (0% and $+\Delta R/R\%$) were assigned to inactive domains (Fig. 1H). The ratio of active domains to inactive domains was 0.76 ± 0.20 ($n = 8$ cats). Average time courses were plotted from all pixels within each ROI (i.e., vessel, tissue, active, and inactive domains) in the single-condition raw activity maps.

Results

Effects of sNP administration on arterial blood pressure and cortical reflected light intensity

A decrease in arterial blood pressure (BP) causes an increase in CBV to keep CBF rather constant (i.e., autoregulation). Thus, the increase in light absorption (decrease in reflected light) induced by the increase in CBV is expected at low BP. To test this prediction, 570-nm reflected light intensities between normal and low BP were compared. Fig. 2 shows continuous recordings of arterial BP (A) and cortical reflected light at 570-nm wavelength (B) during normal BP (left panel) and during low BP, induced by sNP injection (right panel). The sNP reduced MABP, systolic and diastolic blood pressure, and also pulse pressure (difference between systolic and diastolic blood pressures) (compare left and right panels of Fig. 2A and insets). Target MABP during sNP injections was at ~ 45 mm Hg (right panel of Fig. 2A), which may be slightly below the lower limit of CBF autoregulation (Chillon and Baumbach, 2002). Under this condition, vessels are considerably dilated (Kontos et al., 1978), and thus CBV (Schumann-Bard et al., 2005) and total hemoglobin (Ferrari et al., 1992) are increased. In accordance with our expectation, the reflected light intensity gradually decreased from ~ 800 arbitrary units during normal BP to ~ 700 units during low BP (Fig. 2B).

To quantitatively compare properties of reflected light between the two BP conditions, *mean* of the reflected light intensity for a 10-s pre-stimulus period was calculated for each of the selected runs (see OIS data analysis in Materials and methods) for both BP conditions. The mean reflected light intensity of 570-nm wavelength during low BP (MABP, 48.3 ± 5.8 mm Hg) for all five cats was $8.0 \pm 6.7\%$ less than that during normal BP (MABP, 81.2 ± 5.0 mm Hg). Similarly, the average reflected light intensity at 620 nm during low BP (MABP, 48.1 ± 3.3 mm Hg) for all five cats was reduced by $2.2 \pm 1.5\%$, compared to that with normal BP (MABP, 82.1 ± 3.3 mm Hg). The decreases in reflected light intensity were

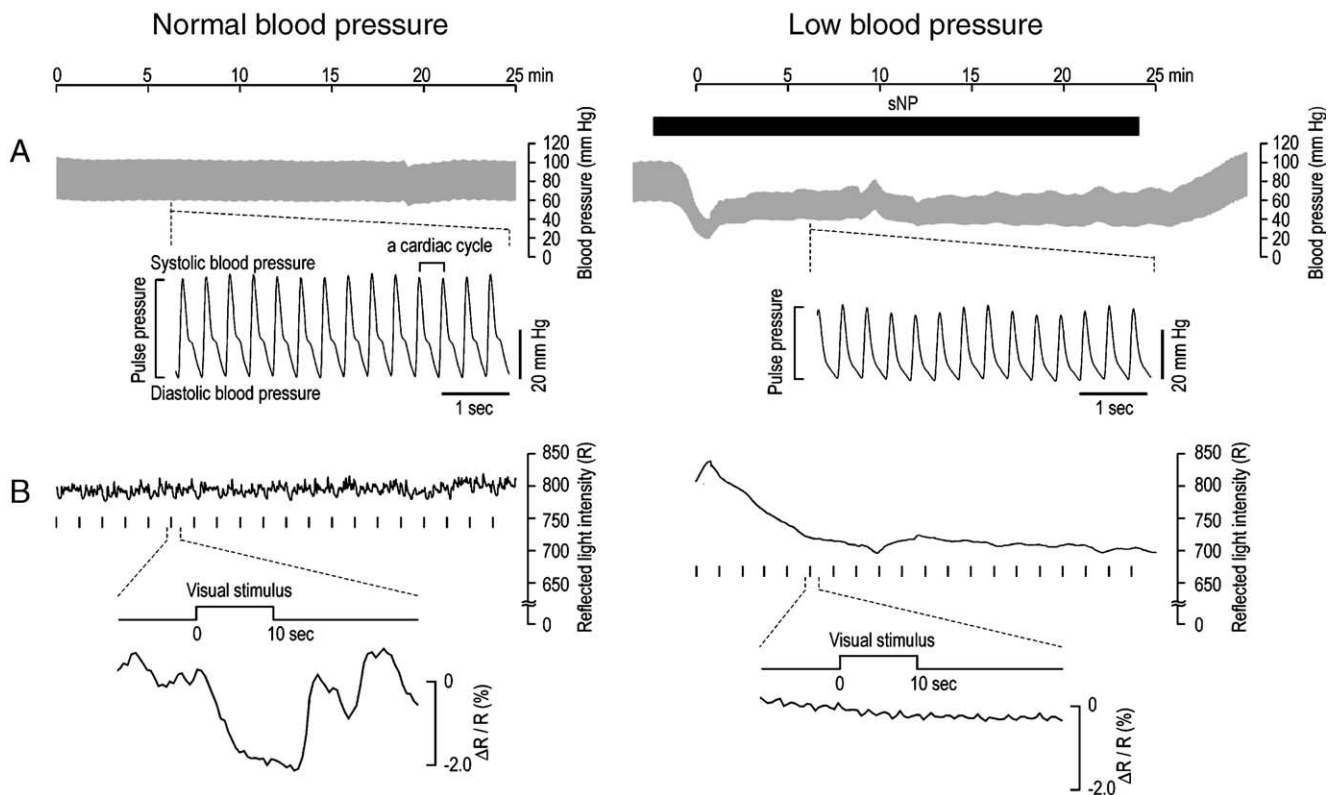


Fig. 2. Effects of sNP administration on BP and cortical reflected light intensity. Continuous recordings of arterial BP and reflected light intensity from the cortex with normal BP (left panels) and those with low BP (right panels) for ~25 min from one study. Time 0 min indicates beginning of OIS recording. (A) Traces of arterial BP. The period of sNP injection is indicated by the horizontal black bar in the right panel. Portions (5 s) of BP traces are expanded to show details in the insets. (B) Traces of reflected light intensity (R) at 570-nm wavelength (obtained from the ROI shown in Figs. 3A and B). The same arbitrary unit is used in both BP conditions. Short vertical bars below the traces indicate the onset of stimulus (grating orientation at 45°). Reflected light is shown as a percentage change ($\Delta R/R$). The smaller 0.5 Hz fluctuations are probably due to CBV modulations synchronized with respiration rate.

statistically significant ($P = 0.046$ for 570 nm and 0.029 for 620 nm). This indicates an increase in CBV induced by the decrease of blood pressure.

The reduction of MABP also lessened the fluctuation in the reflected light intensity. As shown in Fig. 2B, the trace of reflected light intensity during normal BP appeared noisy compared to that for low BP. To quantify the fluctuation within a run, one SD of the reflected light intensity for a 10-s pre-stimulus period (SD) was divided by the mean of reflected light intensity (SD/mean). The average SD/mean for 570-nm wavelength at low BP ($0.14 \pm 0.12\%$, $n = 5$ cats) was significantly smaller ($P = 0.012$) than that at normal BP ($0.74 \pm 0.40\%$). Similarly, the average SD/mean for 620-nm wavelength at low BP ($0.06 \pm 0.02\%$, $n = 5$ cats) was significantly smaller ($P = 0.002$) than that at normal BP ($0.10 \pm 0.03\%$). Since this signal fluctuation is significantly reduced during the low BP condition, smaller stimulation-induced signal changes should be detectable.

Reduction of the stimulus-induced CBV changes during low arterial blood pressure

To evaluate whether the low BP condition can also mitigate the contribution of stimulus-induced CBV changes to OIS, we recorded light reflection changes induced by visual stimulation with 570-nm wavelength (i.e., 570-nm OIS) during both BP conditions. A decrease in light reflection at 570 nm as shown in

single-run traces of Fig. 2B inset was observed for every visual stimulus during normal BP (Fig. 2B left), but the signal changes almost disappeared during the low BP condition (Fig. 2B right). This observation was preserved even after averaging all selected runs (Figs. 3A–F, the same cat as Fig. 2). Cortical surface vessels within the ROI are clearly visible during both BP conditions and are dilated for low BP, as can be seen in the pre-stimulus baseline images of Figs. 3A and B. Visual stimulation induced a decrease in light reflection (i.e., a darkening of the cortical images) over the entire ROI as shown in the “single-condition raw activity map” (see OIS data analysis in Materials and methods) of Fig. 3C for normal BP (MABP, 76.1 ± 0.6 mm Hg, average for 17 runs). These global reflection changes almost disappeared in the activity map for low BP (MABP, 45.5 ± 1.8 mm Hg, average for 12 runs) (Fig. 3D). In accordance with the activity maps, the light reflection change induced by stimulation within both tissue and pial vessel regions (see ROI analysis in Materials and methods) was maximum ~2% for normal BP (Fig. 3E) but was maximum ~0.05% for low BP condition in their time courses (note that the vertical scale in Fig. 3F is ten times smaller than that in Fig. 3E). The reduction of signal reached ~90% after 4 s from the stimulus onset (Fig. 3F inset). This signal reduction during low BP was consistently observed across all five cats (Fig. 3G).

To quantitatively compare the magnitude of the 570-nm OIS between normal and low BP conditions, we separately averaged the reflection changes in the regions of tissue and pial vessels

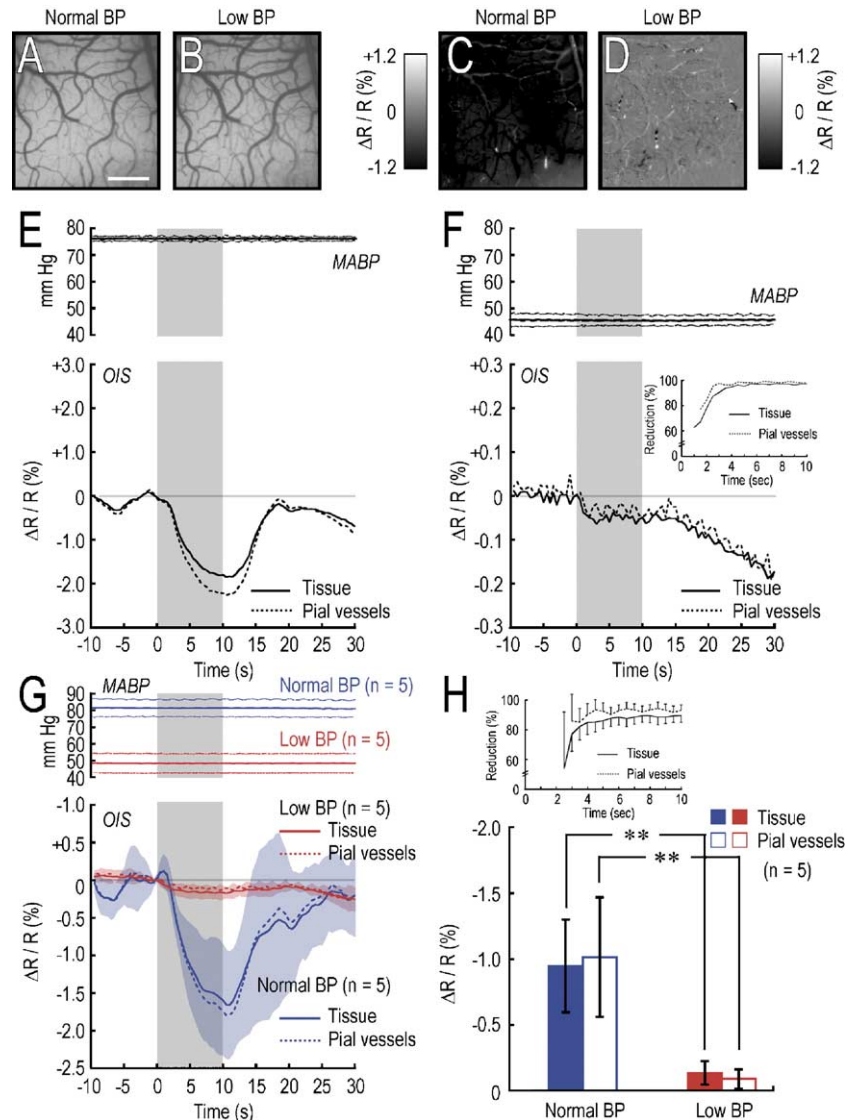


Fig. 3. Reduction of the stimulus-induced CBV changes during low BP. (A–F) Representative data for one cat at 570-nm wavelength. The data are from the same study as Fig. 2. (G and H) Data for all five cats at 570-nm wavelength. (A and B) Images of the cortical surface at baseline during normal (A) and low (B) BP conditions for reference to maps in panels C and D. The scale bar is 1 mm. (C and D) Single-condition raw activity maps for visual stimulation with a grating orientation of 45° during normal (C) and low (D) BP. Data for the maps were averaged from 0.5 to 10 s after stimulus onset. (E and F) (upper panels) Time course of MABP with ± 1 SD. (Lower panels) Average time courses for selected runs for one study of 570-nm OIS during normal (E) and low (F) BP from within the regions shown in panels C and D. Solid and dotted lines depict signal originating from tissue and pial vessels, respectively. In the subsequent figures, the 0 time point represents the onset of stimulus and a gray bar indicates the stimulus presentation period. (Inset in panel F) Signal reduction rates over time (solid line, tissue; dotted line, pial vessels). Initial few seconds were not plotted due to low SNR. (G) (upper panel) Average time course of MABP with ± 1 SD ($n = 5$ cats). (lower panel) Average time courses of 570-nm OIS ($n = 5$ cats) under normal (blue) and low (red) BP. Paler shaded colors indicate ± 1 SD. (H) Average magnitudes of the 570-nm OIS ($n = 5$ cats) from 0 to 10 s after stimulus onset under normal (blue) and low (red) BP conditions. Filled and open bars depict tissue and pial vessels, respectively. Error bars are ± 1 SD. The double asterisk (**) indicates $P < 0.01$. (Inset) Average signal reduction rates for five cats over time (solid line, tissue; dotted line, pial vessels). Initial few seconds were not plotted due to low SNR. Error bars are ± 1 SD.

during 10-s stimulation (from 0.5 s to 10 s after the stimulus onset, 0 s was not included because the signal did not emerge clearly) for each cat (Fig. 3H). Result with two-way repeated measures ANOVA indicated that the difference between magnitudes of reflection change from tissue vs. pial vessels was not statistically significant ($F_{1,16} = 0.007$, $P = 0.936$), while the magnitude difference between normal and low BP was statistically significant ($F_{1,16} = 43.604$, $P < 6.07 \times 10^{-6}$). The average magnitude of the 570-nm OIS from tissue for all five cats significantly decreased

($P = 0.004$) during the low BP conditions ($\Delta R/R$, $-0.14 \pm 0.09\%$; MABP, 48.3 ± 5.8 mm Hg) compared to that with normal BP ($\Delta R/R$, $-0.95 \pm 0.35\%$; MABP, 81.2 ± 5.0 mm Hg), and recovered to a similar magnitude when MABP returned to normal ($\Delta R/R$, $-1.33 \pm 0.40\%$; MABP, 88.7 ± 8.0 mm Hg). Thus, the average 570-nm OIS reduction at low BP was $85.8 \pm 6.1\%$ ($n = 5$ cats). A statistically significant reduction of reflection changes was similarly observed in pial vessels ($\Delta R/R$, $-1.02 \pm 0.45\%$ at normal BP; $\Delta R/R$, $-0.09 \pm 0.08\%$ at low BP, $P = 0.008$). As shown in the time

courses of signal reduction rates (Fig. 3H inset), a similar reduction of the signals was mainly observed in later time points (4–10 s from the stimulus onset). These results are consistent with our expectation that the 570-nm OIS would be considerably reduced by decreasing the BP. This suggests that the 570-nm OIS is predominantly derived from changes in total hemoglobin content (i.e., CBV) as has generally been assumed (for review, see Bonhoeffer and Grinvald, 1996), and thus stimulus-induced CBV changes were greatly reduced under low BP conditions.

Preservation of neural activity during low arterial blood pressure

The reduction of stimulus-induced CBV during low BP is due to a loss of vasodilation capacity or a decrease of neural activity. To test whether a decrease in neural activity is the major source of reduced evoked CBV responses, multiple-spiking activities of neurons were recorded in two cats. Fig. 4A shows examples of spike firing rates of multiple neurons for a 10-s visual stimulation periods during normal (left panel) and low BP (right panel) conditions. Although spiking activity from multiple neurons transiently disappeared for the initial few minutes after the MABP reduction, the activity recovered to the pre-infusion levels. The initial loss of neural activity may be related to hypotension ischemia (Sato et al., 1984) rather than direct sNP effects (see

Discussion); an initial drop of MABP to ~ 40 mm Hg may extremely slow down or stop local blood perfusion at that period. This would cause a decrease in oxygen tension in tissue, leading to a decrease of cerebral metabolic rate of oxygen consumption ($CMRO_2$). Spiking activity only disappeared during initial MABP of ~ 40 mm Hg period and recovered when MABP returned to ~ 45 mm Hg (Fig. 4A). If sNP itself affected spiking activity, the activity would not be recovered during sNP administration. This initial deactivation (~ 5 min) may also be related with the initial unstable light reflectance (see Fig. 2C).

To quantitatively compare the magnitude and selectivity of neural activity between normal BP (control) and low BP conditions, the average spike frequency during 10-s stimulation for 5 runs was calculated for each orientation (0° , 45° , 90° , and 135°) for both BP conditions. As shown in Fig. 4B, orientation tuning at low BP (red lines) was essentially the same as that in normal BP (blue lines). Furthermore, average dynamics of the spike firing rates at preferred and anti-preferred (i.e., orthogonal) orientation was similar between two BP conditions (Fig. 4C, MABP, 95.7 ± 9.0 mm Hg (normal) vs. 47.5 ± 3.2 mm Hg (low), $n = 4$ sites). These data show that neural activity does not change between normal and low BP conditions, and therefore, the significant reduction of 570-nm OIS we observed during low BP conditions is not due to a decrease of neural spiking activity.

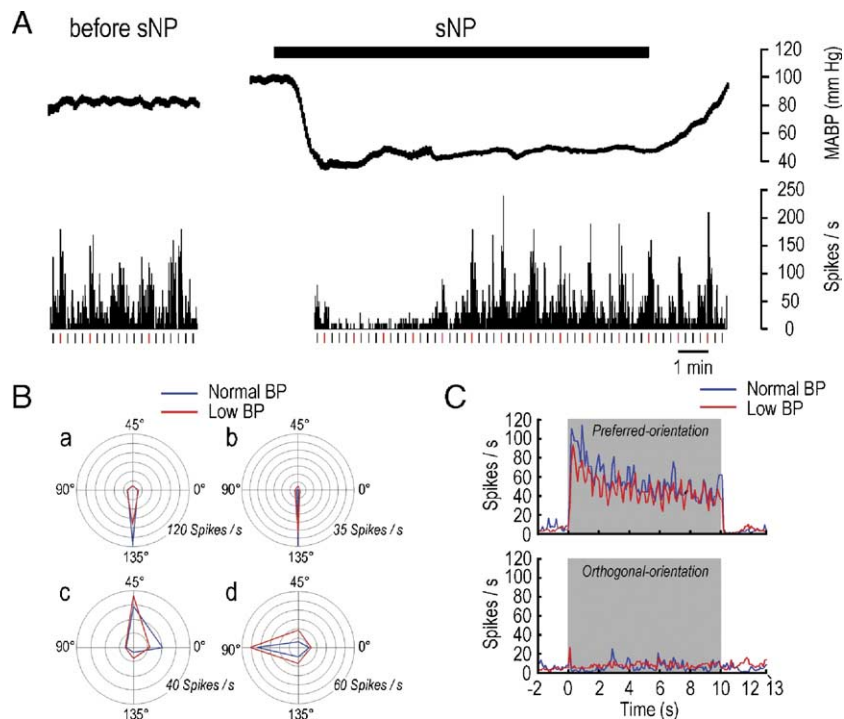


Fig. 4. Preservation of neural activity during low BP. (A) Example of spike activity of multiple neurons induced by a 10-s visual stimulation during normal (left panels) and low BP (right panels); MABP (upper), spike firing rates in 100-ms bins (lower). The period of sNP injection is indicated by the horizontal black bar in the right upper panel. Vertical ticks below the lower traces represent stimulus onset for each run. Runs recorded at the preferred orientation are indicated by red ticks. (B) Orientation tuning curves of all recorded neurons ($n = 2$ cats). Blue and red lines represent the average for 5 runs at normal and low BP, respectively. MABP at each run was determined by averaging the values for 15 s (from 2 s pre-stimulus to 13 s after stimulus onset), yielding normal/low MABP (mm Hg) average values for 5 runs of (a) $100.9 \pm 2.1/52.2 \pm 2.2$, (b) $98.7 \pm 1.8/44.9 \pm 2.9$, (c) $82.3 \pm 1.2/46.6 \pm 2.1$, (d) $100.7 \pm 1.8/46.8 \pm 2.1$. Isocontours indicate the same firing rates (spikes/s). The center is 0 spike/s. The inner iso-contour firing rate can be obtained by dividing the given firing rate by the number of contours. Neurons a and b were recorded from the same penetration track in one cat ($500 \mu\text{m}$ and $300 \mu\text{m}$ below the cortical surface, respectively). Neurons c and d were recorded at two different penetration sites from another cat (both recorded at $300 \mu\text{m}$). Activity shown in panel A is neuron c. (C) Peri-stimulus time histograms in 100-ms bins during normal (blue) and low (red) BP conditions with 10-s visual stimulation, where spike firing rates at preferred (upper panel) and orthogonal (lower panel) orientations for neurons at 4 different sites (a–d in panel B) were averaged.

Enhancement of the dip during low arterial blood pressure

The reduction of CBF and CBV at low BP without a concomitant decrease of neural activity will cause dHb increase to be sustained during stimulation. Thus, the dip in the dHb-weighted 620-nm OIS at low BP is expected to continue during the entire 10-s stimulation period, unlike the 620-nm OIS at normal BP.

Typical spatiotemporal responses of the 620-nm OIS for 10-s stimulation at normal and low BP from one cat are shown as single-condition raw activity maps in Figs. 5A and B, respectively, and as the average time courses from tissue and pial vessels in Fig. 5C. During the normal BP condition (MABP, 81.5 ± 3.8 mm Hg, average for 12 runs), decreases of light reflection induced by visual stimulation were highly localized to patches within ~ 2 s after the stimulus onset (see 1.5 s in Fig. 5A) which is consistent with the previous reports (Grinvald et al., 2000; Malonek and Grinvald, 1996). Afterwards, they quickly spread throughout the cortex (see darkening of the cortical image in the panel of 5.0 s), followed (at normal BP) by a global increase of light reflection (see lightening of the cortex in the panel of 10.0 s). The biphasic time course of the 620-nm OIS at normal BP (blue lines in Fig. 5C) suggests that dHb contents initially increase due to increases in oxygen consumption

by active neurons (Vanzetta and Grinvald, 1999; but see Lindauer et al., 2001), then later decrease due to over-compensation of CBF (Fox and Raichle, 1986). Both tissue and pial vessels behaved similarly at normal BP over the entire time course, and results were consistent in all 5 cats (Fig. 5D). During the low BP conditions (MABP: 51.4 ± 1.4 mm Hg, average for 11 runs), light reflection decreased at 1.5 and 5.0 s (Fig. 5B), similar to normal BP conditions, but a continuing decrease in light reflection (i.e., a prolonged dip) was observed over the cortical region during the entire stimulation period (see 10.0 s in Fig. 5B). The monophasic time courses were observed similarly in both tissue and pial vessels (red lines in Fig. 5C). This was consistent across all five cats (Fig. 5D). The result suggests that a prolonged increase in dHb content is detectable at low BP because the sustained increase in oxygen metabolism is not compensated by further increases in oxygen supply due to CBF and CBV changes (Offenhauser et al., 2005).

To quantitatively compare the dHb signals between normal and low BP conditions, the maximum magnitude of the dip during the 10-s stimulation was determined (time for maximum tissue signal was chosen for both tissue and pial vessels). Result with two-way repeated measures ANOVA indicated that the difference between magnitudes of reflection changes from tissue vs. pial vessels was

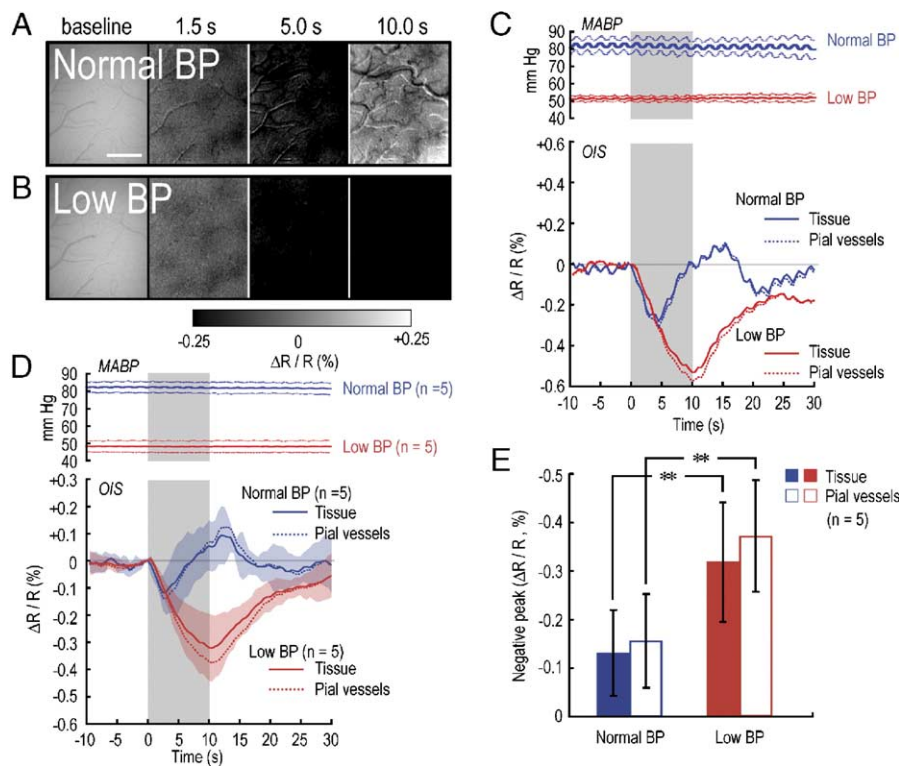


Fig. 5. Enhancement of the dip during low BP. (A–C) Representative data for one cat at 620-nm wavelength. The data are from the same study as Fig. 1. (D and E) Data for all five cats at 620-nm wavelength. (A and B) Images of the cortical surface at baseline (left panels) and single-condition raw activity maps for visual stimulation with a grating orientation of 45° at 1.5, 5.0, and 10 s after stimulus onset during normal (A) and low (B) BP. The cortical surface images were sharpened by Photoshop (Adobe) to enhance vascular patterns. Note that vessels were dilated at low BP. The scale bar is 1 mm. (C) (upper panel) Time courses of MABP with ± 1 SD ($n = 5$ cats). (lower panel) Time courses of the 620-nm OIS from the region shown in panels A and B. Reflection changes from tissue (solid lines) and pial vessels (dotted lines) are plotted for both normal (blue) and low (red) BP. (D) (upper panel) Average time courses of MABP with ± 1 SD. (lower panel) Average time courses of the 620-nm OIS ($n = 5$ cats) with normal (blue lines) and low (red) BP. Solid and dotted lines depict signal from tissue and pial vessels, respectively. Paler shaded colors indicate ± 1 SD. (E) Average magnitudes of the minimum 620-nm OIS ($n = 5$ cats) for normal (blue) and low (red) BP conditions where maximum negative deflections of tissue signal during the 10-s stimulation in individual cats were averaged. Filled and open bars depict signal from tissue and pial vessels, respectively. For calculations, the same time point was chosen for pial vessel signal as for the tissue signal. Error bars are ± 1 SD. The double asterisk (**) indicates $P < 0.01$.

not statistically significant ($F_{1,16} = 0.646$, $P = 0.433$), while the magnitude difference between normal and low BP was statistically significant ($F_{1,16} = 17.499$, $P = 0.001$) (Fig. 5E). In both tissue and pial vessels, the average maximum dip for all five cats with low BP ($\Delta R/R$: $-0.32 \pm 0.12\%$ for tissue, $-0.37 \pm 0.12\%$ for vessels, MABP: 48.1 ± 3.3 mm Hg) was significantly larger ($P = 0.002$ for tissue, $P = 0.0008$ for vessels) than that with normal BP (MABP, 82.1 ± 3.3 mm Hg; $\Delta R/R$, $-0.13 \pm 0.09\%$ for tissue; $-0.16 \pm 0.10\%$ for vessels). The responses recovered when MABP returned to normal (MABP, 84.0 ± 2.0 mm Hg; $\Delta R/R$, $-0.13 \pm 0.03\%$ for tissue; $-0.16 \pm 0.04\%$ for vessels). Similar magnitudes of reflection changes in pial vessel and tissue ROIs suggest that increased dHb in tissue drains to the pial vessels.

Preservation of orientation selectivity of deoxyhemoglobin signals during low arterial blood pressure

Since neural spiking activity was preserved during the low BP condition (see Fig. 4), orientation selectivity of oxygen consumption in neurons is also expected to be the same as it is for normal BP. To test this prediction, we examined selectivity of the 620-nm OIS for normal and low BP because the 620-nm OIS originates mostly from dHb content changes in blood, which can be related to the oxygen consumption by neurons. For this purpose, “single-condition iso-orientation maps” (see OIS data analysis in Materials and methods) were calculated to obtain spatial patterns of the 620-nm OIS specific to a stimulus orientation (Grinvald et al., 1986; Shmuel and Grinvald, 1996); the orientation-non-specific signal is removed from this map. It should be noted that the non-specific signal is usually 5–10 times larger than the orientation-specific signal (e.g., the gray scale range of Figs. 5A and B was five times larger than that of Figs. 6A and B). In a representative study, the spatial pattern of iso-orientation domains (black patches marked with white crosses) with normal BP (Fig. 6A) appears essentially the same as that for low BP (Fig. 6B). The correlation coefficient between two single-condition maps for a corresponding 100×100 -pixel (2.75×2.75 mm², white rectangles in Figs. 6A–D) region (not including pial vessels, the cortical vasculature is shown

in Fig. 6C) was significantly high ($R = 0.62$, $P < 0.01$; for 5 cats $R = 0.51 \pm 0.07$). The location of iso-orientation domains was confirmed by a “differential iso-orientation map” at normal BP (see OIS data analysis in Materials and methods) shown in the Fig. 6D. Negative percentage values (i.e., black patches) in the differential iso-orientation map are referred to as “active domains” and remaining area as “inactive domains” (see also OIS data analysis in Materials and methods).

To determine whether orientation selectivity in 620-nm OIS is preserved at low BP, single-condition iso-orientation maps for one stimulus orientation at both low BP and at normal BP (as a control) obtained from the experiment of *Single-orientation 570 and 620-nm OIS* were compared with differential iso-orientation maps for four stimulus orientations obtained from the experiment of *Four-orientation 620-nm* (for each experiment, see Materials and methods and Table 1) (Fig. 6E). The correlation coefficient was calculated between the single-condition iso-orientation maps and the differential iso-orientation maps for corresponding 100×100 -pixel regions. For the low BP single-condition iso-orientation data, the highest positive correlation was observed when the grating orientation was the same as the differential iso-orientation map (i.e., angular difference, 0°), while the highest negative correlation was detected when orientations were orthogonal (i.e., angular difference, 90°). The difference between normal vs. low BP was not statistically significant (two-way repeated measures ANOVA, $F_{1,4} = 2.364$, $P = 0.199$), suggesting that dHb signals at both normal and low BP show similar orientation selectivity.

Furthermore, we calculated the magnitude difference of the OIS between active and inactive domains, which likely correlate with spike firing rates of neurons in the active domain (Shmuel and Grinvald, 1996). To calculate the magnitude difference in OIS, time courses of the 620-nm OIS in active and inactive domains were separately obtained. Then the signals during 10-s stimulation (from 0.5 to 10 s after the stimulus onset, 0 s was not included because the signal did not emerge clearly) were averaged. The mean magnitude difference between active and inactive domains for the 620 nm OIS ($n = 5$ cats) at normal BP ($0.03 \pm 0.01\%$) was statistically not different ($P = 0.25$) from that with low BP ($0.04 \pm$

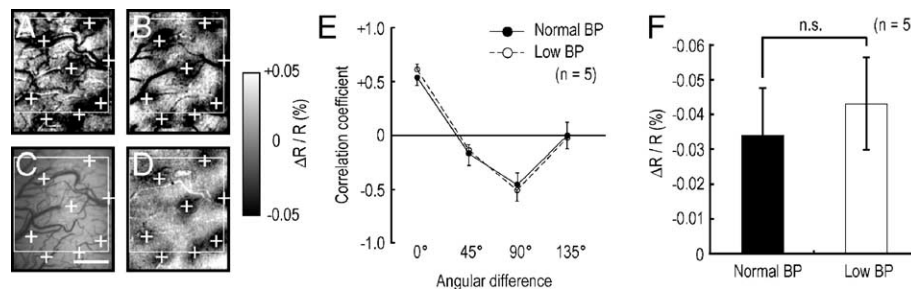


Fig. 6. Preservation of orientation selectivity of dHb signals during low BP. (A and B) Single-condition iso-orientation maps at 620 nm for visual stimulation with a grating orientation of 45° during normal (A) and low (B) BP. Data for the maps were obtained from the *Single-orientation 620-nm OIS* experiment and averaged from 0.5 to 10 s after stimulus onset (during stimulation). The data are from the same study as Figs. 5A and B. Note that global reflection changes were filtered out (see Figs. 1B–E). (C) A cortical surface image at 540 nm shows pial vessels for reference to the maps in panels A, B, and D. The scale bar is 1 mm. (D) Differential iso-orientation map at 620 nm obtained from the *Four-orientation 620-nm OIS* experiment. Black patches in panels A, B, and D are selective responses to the grating at 45° orientation. Locations of the patches were determined on the differential map and marked with white crosses on all images. The white rectangles are the regions (100×100 pixels) for calculating correlation coefficient in this example. (E) Average correlation coefficients ($n = 5$ cats) based comparisons on a pixel to pixel basis. The horizontal axis represents the angular difference of stimulus orientations between the single-condition and the differential iso-orientation data, where single-condition iso-orientation maps were obtained at only one orientation during both normal (filled circles) and low (open circles) BP, and differential iso-orientation maps were obtained at normal BP for four different orientations. 0° indicates that the single-condition vs. differential map comparisons are for identical stimuli, while 90° indicates that the comparisons are for orthogonal orientations. Error bars are ± 1 SD (only one side is plotted). (F) Average magnitude difference (i.e., ‘active domain’ minus ‘inactive domain’). Error bars are ± 1 SD. The n.s. indicates that there was no statistically significant difference ($P = 0.25$, $n = 5$ cats).

0.01%) (Fig. 6F). This similarity of the mean magnitude difference for normal and low BP further demonstrates the preserved orientation selectivity at low BP. Taken together with the similarity of preferred orientation spiking activity for both BP conditions (Fig. 4C), these data suggest that the dHb change in blood measured by 620-nm OIS reflects increases of oxygen consumption in neurons. Thus, spatial specificity inherent in dHb signals can be examined during the low BP condition because only the CBF and CBV responses induced by neural activity are minimized.

Time-dependent spatial specificity of deoxyhemoglobin and CBV signals

To examine the spatial specificity of OIS, we separately calculated time courses of OIS within active and inactive domains from the single-condition raw activity maps (Figs. 7A and B). Whether the stimulus-induced reflection changes at 620 nm were positive or negative, similar magnitudes of reflection changes were observed at all time points in both the active and inactive domains at normal BP (Fig. 7A, red and blue lines in left panel). Interestingly, signal magnitudes of the two domains at 620 nm were similar even at the low BP conditions (Fig. 7A, right panel). Since stimulation-induced changes in blood velocity and volume were reduced significantly during the low BP conditions, the 620-nm OIS observed in both domains is not likely to be due to widespread dHb changes caused by CBF and CBV responses or light scattering (Ls) induced by velocity changes (Tomita et al., 1983), but rather caused by widespread dHb content changes per se. Similar magnitudes of reflection changes in active and inactive domains were also observed at 570 nm (Fig. 7B), where the signal source is CBV weighted. It should be noted that our selection of

active and inactive column ROIs is based on conventional optical imaging approaches. If a higher threshold (such as a z score of 2) is used for the decision of ROIs, the signal difference between the active and inactive ROIs (green lines in Fig. 7) is larger; in present studies, the signal difference between active and in-active domains is the smallest. However, its time-dependent characteristics remain the same.

Before reporting quantitative results of the spatial specificity, the “sensitivity” and “specificity” of the OIS signal have to be defined (see also discussion in Duong et al., 2000a). Fig. 8A shows two hypothetical OIS profiles (S1 and S2, blue and red solid lines respectively) from single-condition raw activity maps, in which two neighboring iso-orientation domains (gray areas in A) are activated simultaneously. OIS activation area is much larger than column size determined by neural spike activity (black bars in A); OIS is induced even in orthogonal orientation columns (between two gray areas in A). Thus, OIS consists of orientation-non-specific and -specific signals. Typically, when two orthogonal stimuli are employed, orientation-non-specific signals have been determined by cocktail blank analysis. Analogous to this, the orientation-non-specific component is obtained from an average of signals between the iso-orientation and orthogonal domains (DC₁ and DC₂, blue and red dotted lines respectively). “Sensitivity” to detect a column is determined by the magnitude of the orientation-specific modulations (ΔS_1 and ΔS_2). To compare the sensitivity of S1 and S2, the orientation-non-specific modulations (DC₁ and DC₂) are subtracted from the raw OIS profiles (S1 and S2). As in Fig. 8B, the S1 sensitivity is larger than the S2 ($\Delta S_1 > \Delta S_2$). However, larger sensitivity does not necessary mean better spatial specificity; the non-specific modulation should also be considered. The “specificity” of the signal is related to the signal point spread, which is generally determined by the full-width at half-maximum (FWHM) of the signal. To compare the FWHM of the S1 and S2, each with different magnitude, the peak of S1 and S2 is normalized to 1.0. As in Fig. 8C, the profile of the S1 is broader than that of the S2. Thus, the FWHM of the S2 (a red horizontal bar) is smaller than that of the S1 (a blue horizontal bar); the specificity of the S2 is better than that of the S1. Instead of FWHM, the normalized sensitivity ($\Delta S'_1$ and $\Delta S'_2$) can be used as an index of FWHM because it is correlated with FWHM (i.e., $\Delta S'_1 < \Delta S'_2$; larger value, better specificity). However, normalization by the signal peak is not practical for the OIS raw activity maps because signal magnitudes are different among iso-orientation domains (e.g., see Fig. 8G). Thus, we used the orientation-non-specific signal for normalization instead (Fig. 8D); the orientation-specific modulation (Fig. 8B) is divided by the non-specific modulation (DC₁ and DC₂ in Fig. 8A). We will refer to this ratio ($\Delta S/DC$) as spatial specificity index (larger ratio, better specificity). As consistent to the Fig. 8C ($\Delta S'_1 < \Delta S'_2$), the spatial specificity index of the S2 is larger than that of the S1 ($\Delta S_1/DC_1 < \Delta S_2/DC_2$), suggesting better spatial specificity of the S2 compared to the S1 (Fig. 8D).

Actual OIS profiles (a 620-nm OIS with low BP) corresponding to Figs. 8A–D are shown in Figs. 8E–H. OIS profiles from single-condition raw activity maps at three different time periods (average for 1–2, 4–6, and 8–10 s) were plotted in Fig. 8E (thick solid lines, raw signals; thin solid lines, low-pass filtered (cutoff frequency, 1.5 Hz) signals). Dotted lines are the orientation-non-specific modulations, which were obtained from “single-condition raw activity maps” minus “single-condition iso-orientation maps”. The arrow indicates the location of a column (see Fig. 9A). Both orientation-

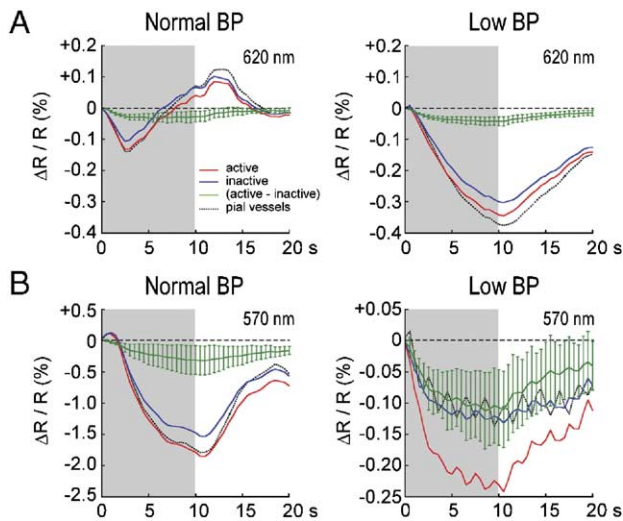


Fig. 7. Time courses of dHb and CBV signals from active and inactive domains. (A) Average time courses of the 620-nm OIS ($n = 5$ cats) for normal (left panel) and low (right panel) BP conditions. The red and blue lines depict reflection changes for active and inactive domains, respectively. The green line represents changes in ‘active domain’ (red line) minus changes in ‘inactive domain’ (blue line). The black dotted line indicates the reflection changes in pial vessels. Error bars of green lines are ± 1 SD. (B) Average time courses of the 570-nm OIS ($n = 5$ cats) for normal BP (left panel) and low BP (right panel) conditions. Color representations are the same as for panel A.

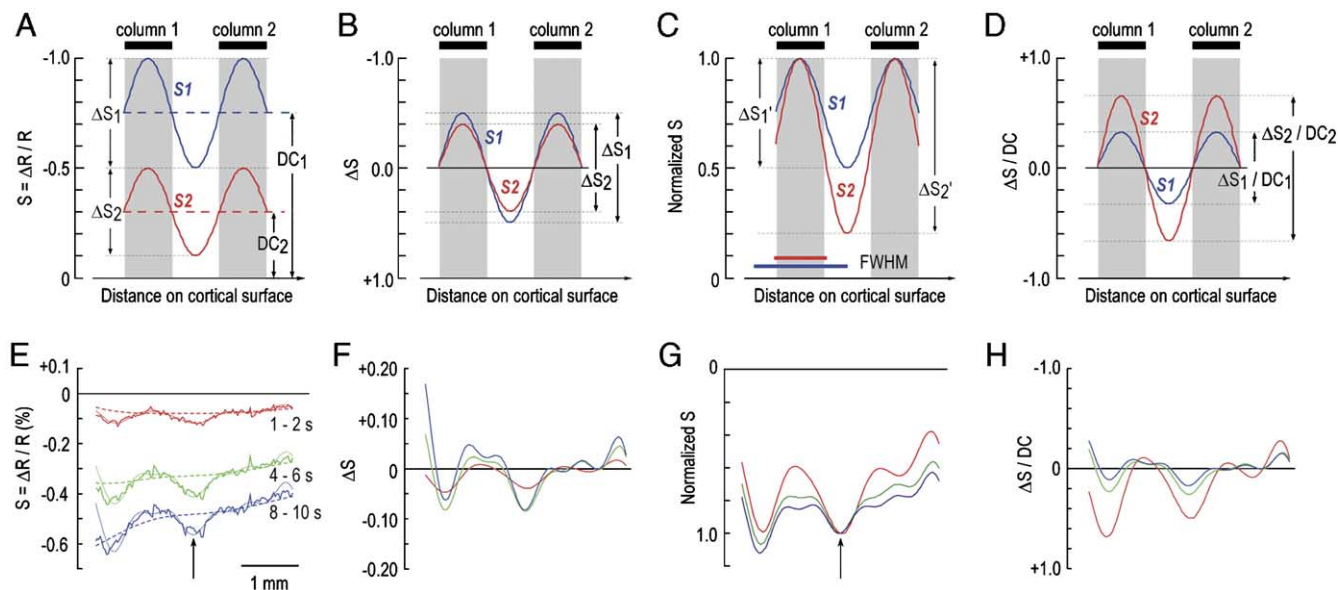


Fig. 8. Definition of sensitivity and specificity. (A–D) OIS profiles from hypothetical data. (E–H) OIS Profiles corresponding to panels (A–D) from actual data (620-nm OIS with low BP) obtained from the region between two dashed lines in Fig. 9A. (A) Two OIS profiles (solid blue (S1) and red (S2) lines) obtained from hypothetical single-condition raw activity maps. Dotted blue and red lines are orientation-non-specific modulations of each OIS. Gray areas are the column size determined by neural spike activity (black bars). (B) Orientation-specific modulation parts (ΔS_1 and ΔS_2) are extracted from the raw OIS signals (S1 and S2) by subtracting the orientation-non-specific modulations (DC_1 and DC_2). (C) Normalized raw OIS profiles. The raw OIS profiles shown in panel A (S1 and S2) are normalized by their peak values in the iso-orientation domains (gray areas). Horizontal blue and red bars are the FWHM of S1 and S2, respectively. After normalization, $\Delta S_1'$ and $\Delta S_2'$ can be used as an index for the FWHM of S1 and S2. (D) Normalized orientation-specific modulations. The orientation-specific modulations shown in panel B (ΔS_1 and ΔS_2) are normalized by the non-specific modulations (DC_1 and DC_2). This ratio ($\Delta S/DC$) is referred to as spatial specificity index. (E) Profiles of single-condition raw activity maps from 620-nm OIS with low BP at three different time periods (1–2 s, 4–6 s, and 8–10 s, red, green, and blue respectively). Thin solid lines superimposed on raw signals (thick solid lines) are OIS profiles after removing high frequency noise by a filter (cutoff 1.5 Hz), which are used for analyses in panels F–H. Dotted lines indicate orientation-non-specific modulations. The arrow indicates the location of an iso-orientation domain. The scale bar and the line colors are applicable to panels E–H. (F) Profiles of orientation-specific modulation parts. (G) Profiles of OIS normalized by a peak indicated by the arrow. (H) Profiles of the orientation-specific modulation parts (F) normalized by the orientation-non-specific components (dotted lines in panel E).

non-specific (dotted lines in Fig. 8E) and -specific (Fig. 8F) modulations developed with time. To compare FWHM of the raw OIS signals, the peak of all three profiles indicated by the arrow was normalized to 1.0 (Fig. 8G). In the normalized profiles, the spread of OIS became larger with time. In accordance with this, the spatial specificity index ($\Delta S/DC$) became smaller over time (Fig. 8H).

The maps corresponding to Figs. 8F (sensitivity) and H (spatial specificity index) are shown in upper and lower panels in Fig. 9A, respectively. The sensitivity map is equivalent to the single-condition iso-orientation map (i.e., the orientation-non-specific signal is removed). The specificity index map is obtained from dividing the sensitivity map by an orientation-non-specific map (i.e., the “single-condition raw activity map” minus the “single-condition iso-orientation map”). Higher contrasts of iso-orientation domains in sensitivity and specificity index maps indicate higher sensitivity and specificity, respectively. As in upper panels of Fig. 9A, the iso-orientation domains in the sensitivity maps were clearer in later time points, suggesting the sensitivity became larger with time. On the other hand, the iso-orientation domains in the spatial specificity index maps (Fig. 9A lower panels) were clearer at an early time point (1–2 s) compared to later time points (4–6 and 8–10 s), suggesting the spatial specificity became poor with time. Pial draining vessels' responses were also apparent at later time points. For comparison, sensitivity and specificity index maps for a 570-nm OIS with low BP are shown in upper and lower panels of Fig. 9B. As similar to the 620-nm OIS with low BP, the signal

sensitivity changed with time: it improved. In contrast, the spatial specificity index of the 570-nm OIS with low BP did not seem to change much over time. Pial draining vessels' responses were also not apparent even at later time points.

We finally quantify the average spatial specificity index for 620-nm OIS ($n = 5$ cats) and for 570-nm OIS ($n = 4$ of 5 cats, one cat was excluded from the analysis because of low SNR) at each time point and plot them as a function of time from the stimulus onset (Fig. 10). Since multiple components probably contribute to the OIS at normal BP, each with a different sensitivity and specificity, we only quantified the sensitivity and specificity of OIS at low BP. To obtain the index, the difference in OIS magnitudes between the active and inactive domains (corresponding to the sensitivity (ΔS); green lines in Figs. 7A and B) was divided by the average in OIS magnitude between the active and inactive domains (corresponding to the orientation-non-specific component (DC)). Thus, when the signal is only observed in the active domains, the index will be 2.0. On the other hand, when the magnitude of the signal in the active domains is the same as that in the inactive domains, the index will be 0. Results with one-way repeated measures ANOVA indicated a statistically significant difference among times during a 10-s visual stimulation ($F_{18,72} = 8.122$, $P = 3.73 \times 10^{-11}$) for the 620-nm OIS. During the low BP condition, the average spatial specificity index of the 620-nm OIS for all five cats (red line in Fig. 10A) was initially as high as 0.86 ± 0.60 (at 1.0 s after the stimulus onset) and quickly declined with time (statistically significant differences between the indices at

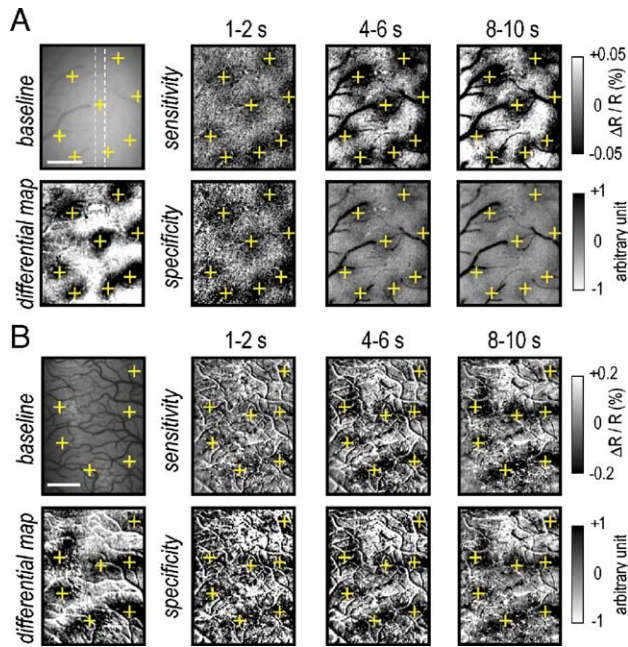


Fig. 9. Sensitivity and spatial specificity index maps at progressive time points. (A) Spatiotemporal patterns of the low BP 620-nm OIS from an illustrative study. A cortical surface image at 620 nm (baseline image) shows pial vessels for sensitivity maps (upper) and spatial specificity index maps (lower) for a 10-s visual stimulation with a grating orientation of 45° at 1–2, 4–6, and 8–10 s from stimulus onset. The scale bar is 1 mm. The data are from the same study as Figs. 8E–H. Yellow crosses on the panels indicate location of black patches selective to the 45° orientation, which were determined from the differential iso-orientation map at 620 nm (differential map). Specificity indices were 0.28, 0.11, and 0.07, while sensitivities were 0.02, 0.04, and 0.04% at progressive time points. (B) Spatiotemporal patterns of the low BP 570-nm OIS from an illustrative study. Specificity indices were 0.66, 0.63, and 0.53, while sensitivities were 0.06, 0.12, and 0.12% at progressive time points. Stimulus orientation used was 0° . Wavelength used was 570 nm except the differential map (620 nm). Other conventions are the same as panel A.

two successive times were $P = 0.001–0.049$). This spatial specificity dependence on time cannot be explained by the scattering of light, which is inherent in optical measurement (Orbach and Cohen, 1983), because scattering of light originating from the active domains to inactive domains should be closely correlated, resulting in time-independent spatial specificity. By contrast, the index of the 570-nm OIS with low BP (blue line in Fig. 10A) did not show such a time variance during a 10-s visual stimulation (results with one-way repeated measures ANOVA indicated no statistically significant difference among times ($F_{18,72} = 0.482$, $P = 0.955$). On the other hand, the sensitivity of the 620-nm OIS during low BP (green line in Fig. 10B) became better at later time points, whereas the specificity became poor (orange line in Fig. 10B). To visualize iso-orientation domains, there is a trade off between the specificity and the sensitivity; specificity is high while sensitivity is poor or vice versa.

Discussion

We have demonstrated during low BP conditions (i) the stimulus-induced CBV response is reduced without changing neural activity, and (ii) time-dependent spatial specificity of dHb

responses to active orientation-selective columns. During visual stimulation under sNP-induced low BP conditions with vessel dilation, the dHb content change (620-nm OIS) resulting from the increase in oxygen consumption can be separated from the effect of CBF and CBV changes (570-nm OIS). Consequently, a prolonged dip was observed in the 620-nm OIS during a 10-s stimulation period. A similar observation was found in fMRI studies in this laboratory (Nagaoka et al., 2002, *in press*), where positive BOLD signals during normal BP conditions changed into negative BOLD signals at low BP. Thus, current dHb-weighted 620-nm and CBV-weighted 570-nm OIS studies are directly applicable to the investigation of spatial specificity of fMRI at a columnar level.

Utilization of sNP-induced low blood pressure

The sNP is widely clinically used to reduce blood pressure. Even at less than 50 mm Hg MABP, the following physiological parameters were well maintained; cortical surface oxygen tension (Maekawa et al., 1979 (cat)), CMRO₂ (Michenfelder and Milde, 1988 (dog); Pinaud et al., 1989 (human); Schumann-Bard et al., 2005; Schumann et al., 1998 (baboon)), pH and normal ionic concentration gradients across cell membranes (Morris et al., 1983 (cat)), evoked field potential (Kottenberg-Assemacher et al., 2003 (human)), and the power of EEG (Ishikawa and McDowall, 1980 (cat)). Here, we have also demonstrated good maintenance of orientation-specific spiking activity (see Fig. 4) and dHb signal (see Fig. 6) during sNP-induced low BP. The reduction of evoked-CBV (the present study) and CBF (Artru and Colley, 1984; Gregory et al., 1981) during sNP-induced low BP seems to be larger than those caused by nitric oxide synthetase (NOS) inhibitors (e.g., Offenhauser et al., 2005; for review, see Iadecola and Niwa, 2002). Thus, instead of use of NOS inhibitors, sNP-induced low BP can be used for a considerable reduction of evoked CBV and CBF responses without concomitant decrease of neural activity.

One concern for sNP administration is cyanide toxicity. However, McDowall et al. (1974) reported no toxicity (i.e., “the animals showing a normal response”) for baboon in the use of $1.25 \text{ mg}\cdot\text{kg}^{-1}\cdot\text{h}^{-1}$ (Table 2 in McDowall et al., 1974). Similarly, cyanide toxicity does not seem to be represented in cat at $<1 \text{ mg}/\text{kg}$ sNP administration (Ishikawa and McDowall, 1980; Maekawa et al., 1979; Morris et al., 1983). Because our total dosage of sNP was

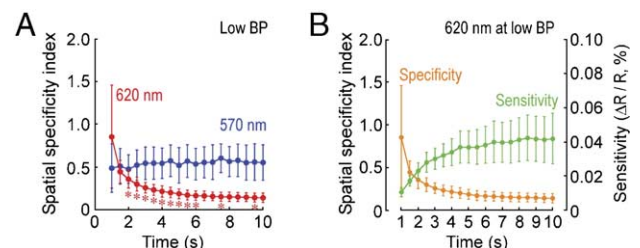


Fig. 10. Time-dependent spatial specificity and sensitivity of dHb and CBV signals. (A) Average time courses of spatial specificity index for the 570-nm (blue) and 620-nm OIS (red) in low BP conditions. The indices at 0 and 0.5 s were not calculated due to poor SNR. Error bars are ± 1 SD ($n = 5$ for the 620-nm OIS; $n = 4$ for the 570-nm OIS). Asterisks (*) indicate a statistically significant difference ($P < 0.05$) between two successive time points. (B) Spatial specificity index (orange line) vs. sensitivity (green line) for 620-nm OIS during low BP. The data in panel A (red line) and Fig. 7A (green line) are used for demonstration. Error bars are ± 1 SD.

less than 1 mg/kg, cyanide toxicity in our preparation may not be significant. Another concern is that nitric oxide (NO) is generated from sNP administration. Because in addition to its vasodilation effect, NO also inhibits cytochrome oxidase (Brown and Cooper, 1994) and thus during sNP administration CMRO₂ is possibly reduced despite unchanged spiking activity. Maekawa et al. (1979) reported a modest decrease of CMRO₂ even in an adequate oxygen supply during sNP-induced low BP. However, even if CMRO₂ decreases during sNP administration, as long as dHb is produced by oxygen consumption, time-dependent spatial specificity of dHb signal should be preserved.

What makes spatial specificity of deoxyhemoglobin signals poor?

The aim of this study was to determine spatial specificity of the dHb signal inherently induced by oxygen consumption. Even though the effect of CBF and CBV changes on the dHb signal was considerably reduced, the spatial specificity of 620-nm OIS to the iso-orientation domains was good only during the initial few seconds (see Figs. 9 and 10). This finding suggests that the poor spatial specificity of the dHb signal at later time points during the low BP condition is not due to widespread dHb changes caused by CBF or CBV modulations but is rather caused directly by widespread changes in the dHb signal itself. Two possible explanations could account for the time-dependent decrease in spatial specificity of the dHb signal at low BP.

First, if the wide extent of the OIS is tied to the wide distribution of sub-threshold synaptic activity (Grinvald et al., 1994; Sharon and Grinvald, 2002) or lateral spread of spiking activity along dendrites and axonal processes, the spatial specificity of the dHb signal will be poor. Since OIS signals are elicited by changes in spiking activity or synaptic potentials of neurons (Das and Gilbert, 1995; Gurden et al., 2003; Kinoshita et al., 2003; Toth et al., 1996) or both, it is plausible that the spread of neural activity over time could cause a time-dependent spread of intrinsic signals (for example, see Liu et al., 2003). Further studies are necessary to determine the neural origin of OIS.

Second, we propose that draining of dHb from active sites can easily explain the time-dependent spread of the 620-nm OIS at low BP. Even though neural origin of the OIS remains controversial, changes in oxygen consumption and glucose metabolism seem to occur within the active iso-orientation domain and not the inactive domain (Lowel et al., 1987; Thompson et al., 2003). Then dHb produced by oxygen consumption increases within active domains should drain into downstream vessels, including intracortical and pial veins, due to the existence of blood flow even though a stimulation-evoked CBF change is not induced (referred to draining effect).

For image detection of the draining effect, the distance between intracortical veins must be less than the size of the functional column. Density of emerging veins ($\sim 2.5/\text{mm}^2$; inter-vessel distance, ~ 0.6 mm, estimated by Fig. 63 in Duvernoy et al. (1981) and Park et al., 2005) is approximately two times higher than that of iso-orientation domains ($\sim 1.2/\text{mm}^2$, inter-columnar distance: ~ 1.0 mm) for a single orientation (Bonhoeffer and Grinvald, 1993; Rao et al., 1997). If dHb induced by neural activity initially increases within active iso-orientation domains and then drains into the intracortical emerging veins, dHb-based signals may not originate from the 'true' active domains. Furthermore, pial venous networks are highly dense, suggesting that dHb changes will eventually spread over the cortical surface, and reducing the

signal specificity further. Consequently, the 620-nm OIS at low BP would lose its specificity with time.

Dynamic 620-nm OIS changes in tissue and in pial vessels were almost identical (see Fig. 5D). This suggests that the draining of dHb from active domains into the pial vessels is faster than our sampling rate (0.5 s). Taking into account that the arteriovenous transit time of red blood cells is 0.1–0.35 s (Hudetz, 1997; Rovainen et al., 1993 in rodents), dHb changes in tissue regions will be quickly integrated into an emerging vein and spread into pial veins within 1 s (see also Narayan et al., 1994; Takashima et al., 2001). Thus, only the early time point (up to ~ 2 s) of the 620-nm OIS dip is specific to active regions.

Spatial specificity of CBV-weighted signals

At normal BP conditions, local CBV changes elicited by neural activity have to occur in concert with dilation in upstream parent arteries (Erinjeri and Woolsey, 2002; Iadecola et al., 1997). To reduce the less-specific vascular contributions from upstream arteries, post-processing analyses were applied to CBV-weighted OIS studies of rodent barrel cortex (Hess et al., 2000; Sheth et al., 2004), and cat and primate visual cortex (Vanzetta et al., 2004). Then CBV changes in parenchymal microvessels (diameter $< \sim 10$ μm) were found to be specific to sub-millimeter functional domains (Frostig et al., 1990; Fukuda et al., 2005; Hess et al., 2000; Narayan et al., 1995; Sheth et al., 2004; Vanzetta et al., 2004). After this removal of signal contribution from pial arteries, CBV-weighted signals originate from penetrating arterioles, branching small arterioles and possibly capillaries. If penetrating arterioles are individually controlled, their density defines the limit for CBV-weighted spatial resolution. The density of penetrating arterioles ($15.8/\text{mm}^2$, inter-arteriole distance: ~ 0.25 mm) in the cat cerebral cortex (McHedlishvili and Kuridze, 1984) is much higher than that of iso-orientation domains ($1.2/\text{mm}^2$, inter-domain distance: ~ 1.0 mm). Thus, detection of penetrating arterioles would provide sufficient resolution for mapping iso-orientation domains in cats. If CBV regulation occurs within smaller-size vessels including capillaries, then an even higher spatial resolution can be achieved.

Reducing arterial BP decreased the less-specific vascular contributions from upstream arteries. The 570-nm OIS almost disappeared at low BP except for a component highly localized to iso-orientation domains (see Fig. 9B). We suggest that this remaining component is also due to CBV changes in parenchymal microvessels rather than changes in Ls due to cellular swelling (Holthoff and Witte, 1996; MacVicar and Hochman, 1991) because the activity-dependent Ls component is unlikely to significantly contribute to the OIS in vivo (Nomura et al., 2000). Since, unlike pial vessels, parenchymal vessels may not be fully dilated at low BP, they can still respond to stimulus (for CO₂ stimulation, see Gregory et al., 1981), suggesting CBV regulation within parenchymal microvessels independently of parent artery.

Implication for columnar resolution functional MRI

Our results suggest that the draining effect of pial and intracortical veins in dHb-based imaging techniques is intrinsically unavoidable (Figs. 5 and 7; see also Hayashi et al., 2005) and reduces its spatial specificity of dHb signal (Figs. 9 and 10); it appears immediately after the stimulus onset (~ 2 s) and becomes dominant with time. Similarly, Duong et al. (2000a) reported that

only the first ~2 s of the entire early negative BOLD response at normal BP showed high spatial specificity to cats' iso-orientation columns; Kim et al. (2000a) used the first 2-s BOLD dip for mapping iso-orientation domains in cats. Positive BOLD data acquired before the draining effect become significant (e.g., less than 2–4 s from stimulus onset) was shown to improve spatial specificity (Goodyear and Menon, 2001; Menon and Goodyear, 1999). Thus, regardless of the BOLD signal polarity (negative or positive), only data obtained within a few seconds after the onset of stimulation (i.e., before the draining effect dominates) can be used for high-resolution studies if the non-specific signal from pial and intra-cortical draining vessels is not removed. Once the non-specific signal is removed, a longer stimulation duration can be applied to increase the sensitivity of signals (i.e., difference between active and inactive domains) (Fig. 8D, see also Cheng et al., 2001).

To reduce the non-specific signals and consequently improve the spatial specificity in primary visual cortex where the cortical modules from orthogonal stimuli have a complementary pattern (e.g., ocular dominance and iso-orientation domains), the non-specific components in optical imaging studies have been removed by (i) the subtraction of imaging signals in response to orthogonal stimuli (Blasdel, 1992; Blasdel and Salama, 1986; Grinvald et al., 1986; for review, see Bonhoeffer and Grinvald, 1996), and (ii) Fourier analysis of data acquired during repeated orthogonal stimuli (Kalatsky and Stryker, 2003). Similar approaches were used to map human ocular dominance columns with positive BOLD (Cheng et al., 2001; Menon et al., 1997). However, the differential methods cannot be applied to most brain areas because orthogonal stimulation condition is unknown. Thus, the single-condition map has to be used.

Positive BOLD signal at normal BP is derived from a mismatch between CMRO₂ and CBF changes. Thus, besides the draining effect, the specificity and sensitivity of BOLD signal are determined by a combination of CMRO₂ and CBF responses. Since an increase in CMRO₂ causes a decrease in BOLD signal, while an increase in CBF causes an increase in BOLD signal, the specificity and sensitivity of BOLD signal are possibly poorer than that of either CMRO₂ or CBF signals (see also Duong et al., 2000a). Thus, alternative non-BOLD fMRI methods, which have high sensitivity and are free from complication by the draining effect, should be considered for single-condition stimulation. Based on our 570-nm OIS results, we suggest that CBV-weighted fMRI (Belliveau et al., 1991; Kennan et al., 1998; Mandeville et al., 1998; van Bruggen et al., 1998) and possibly CBF-weighted fMRI (Edelman et al., 1994; Kim, 1995; Kwong et al., 1992) will have an improved spatial specificity of hemodynamic signals. Unlike the 570-nm OIS, both CBV- and CBF-weighted fMRI can minimize the contribution of large pial vessels even at normal BP (Duong et al., 2000b; Mandeville and Marota, 1999; Silva et al., 2000) and have been successfully applied to laminar (Harel et al., 2002b; Duong et al., 2000b; Lu et al., 2004; Zhao et al., 2004b) and columnar resolution fMRI studies (Duong et al., 2001; Zhao et al., 2005) in the cat visual cortex.

Acknowledgments

We thank Kristy Hendrich, Michelle Tasker, and Toshihiro Hayashi for their helpful comments on the manuscript. This study was supported by NIH EB003324, EB003375, EB002013, NS44589 and McKnight Foundation.

References

- Artru, A.A., Colley, P.S., 1984. Cerebral blood flow responses to hypocapnia during hypotension. *Stroke* 15 (5), 878–883.
- Belliveau, J.W., Kennedy Jr., D.N., McKinstry, R.C., Buchbinder, B.R., Weisskoff, R.M., Cohen, M.S., Vevea, J.M., Brady, T.J., Rosen, B.R., 1991. Functional mapping of the human visual cortex by magnetic resonance imaging. *Science* 254 (5032), 716–719.
- Bishop, P.O., Kozak, W., Vakkur, G.J., 1962. Some quantitative aspects of the cat's eye: axis and plane of reference, visual field co-ordinates and optics. *J. Physiol.* 163, 466–502.
- Blasdel, G.G., 1992. Differential imaging of ocular dominance and orientation selectivity in monkey striate cortex. *J. Neurosci.* 12 (8), 3115–3138.
- Blasdel, G.G., Salama, G., 1986. Voltage-sensitive dyes reveal a modular organization in monkey striate cortex. *Nature* 321 (6070), 579–585.
- Bonhoeffer, T., Grinvald, A., 1993. The layout of iso-orientation domains in area 18 of cat visual cortex: optical imaging reveals a pinwheel-like organization. *J. Neurosci.* 13 (10), 4157–4180.
- Bonhoeffer, T., Grinvald, A., 1996. Optical imaging based on intrinsic signals: the methodology. In: Toga, A.W., Mazziotta, J.C. (Eds.), *Brain Mapping: The Methods*. Academic, San Diego, pp. 55–97.
- Bonhoeffer, T., Kim, D.S., Malonek, D., Shoham, D., Grinvald, A., 1995. Optical imaging of the layout of functional domains in area 17 and across the area 17/18 border in cat visual cortex. *Eur. J. Neurosci.* 7 (9), 1973–1988.
- Brown, G.C., Cooper, C.E., 1994. Nanomolar concentrations of nitric oxide reversibly inhibit synaptosomal respiration by competing with oxygen at cytochrome oxidase. *FEBS Lett.* 356 (2–3), 295–298.
- Buxton, R.B., 2001. The elusive initial dip. *NeuroImage* 13 (6 Pt. 1), 953–958.
- Cheng, K., Waggoner, R.A., Tanaka, K., 2001. Human ocular dominance columns as revealed by high-field functional magnetic resonance imaging. *Neuron* 32 (2), 359–374.
- Chillon, J.-M., Baumbach, G.L., 2002. Autoregulation: arterial and intracranial pressure. In: Edvinsson, L., Krause, D.N. (Eds.), *Cerebral Blood Flow and Metabolism*, 2nd ed. Lippincott Williams and Wilkins, Philadelphia, pp. 395–412.
- Das, A., Gilbert, C.D., 1995. Long-range horizontal connections and their role in cortical reorganization revealed by optical recording of cat primary visual cortex. *Nature* 375 (6534), 780–784.
- Duong, T.Q., Kim, D.S., Ugurbil, K., Kim, S.G., 2000a. Spatiotemporal dynamics of the BOLD fMRI signals: toward mapping submillimeter cortical columns using the early negative response. *Magn. Reson. Med.* 44 (2), 231–242.
- Duong, T.Q., Silva, A.C., Lee, S.P., Kim, S.G., 2000b. Functional MRI of calcium-dependent synaptic activity: cross correlation with CBF and BOLD measurements. *Magn. Reson. Med.* 43 (3), 383–392.
- Duong, T.Q., Kim, D.S., Ugurbil, K., Kim, S.G., 2001. Localized cerebral blood flow response at submillimeter columnar resolution. *Proc. Natl. Acad. Sci. U. S. A.* 98 (19), 10904–10909.
- Duvernoy, H.M., Delon, S., Vannson, J.L., 1981. Cortical blood vessels of the human brain. *Brain Res. Bull.* 7 (5), 519–579.
- Edelman, R.R., Gaa, J., Wedeen, V.J., Loh, E., Hare, J.M., Prasad, P., Li, W., 1994. In vivo measurement of water diffusion in the human heart. *Magn. Reson. Med.* 32 (3), 423–428.
- Endrich, B., Franke, N., Peter, K., Messmer, K., 1987. Induced hypotension: action of sodium nitroprusside and nitroglycerin on the microcirculation. A micropuncture investigation. *Anesthesiology* 66 (5), 605–613.
- Erinjeri, J.P., Woolsey, T.A., 2002. Spatial integration of vascular changes with neural activity in mouse cortex. *J. Cereb. Blood Flow Metab.* 22 (3), 353–360.
- Ferrari, M., Wilson, D.A., Hanley, D.F., Traystman, R.J., 1992. Effects of graded hypotension on cerebral blood flow, blood volume, and mean transit time in dogs. *Am. J. Physiol.* 262 (6 Pt. 2), H1908–H1914.

- Fox, P.T., Raichle, M.E., 1986. Focal physiological uncoupling of cerebral blood flow and oxidative metabolism during somatosensory stimulation in human subjects. *Proc. Natl. Acad. Sci. U. S. A.* 83 (4), 1140–1144.
- Frostig, R.D., Lieke, E.E., Ts'o, D.Y., Grinvald, A., 1990. Cortical functional architecture and local coupling between neuronal activity and the microcirculation revealed by in vivo high-resolution optical imaging of intrinsic signals. *Proc. Natl. Acad. Sci. U. S. A.* 87 (16), 6082–6086.
- Fukuda, M., Rajagopalan, U.M., Homma, R., Matsumoto, M., Nishizaki, M., Tanifuji, M., 2005. Localization of activity-dependent changes in blood volume to submillimeter-scale functional domains in cat visual cortex. *Cereb. Cortex* 15 (6), 823–833.
- Goodyear, B.G., Menon, R.S., 2001. Brief visual stimulation allows mapping of ocular dominance in visual cortex using fMRI. *Hum. Brain Mapp.* 14 (4), 210–217.
- Gregory, P., Ishikawa, T., McDowall, D.G., 1981. CO₂ responses of the cerebral circulation during drug-induced hypotension in the cat. *J. Cereb. Blood Flow Metab.* 1 (2), 195–201.
- Grinvald, A., Lieke, E., Frostig, R.D., Gilbert, C.D., Wiesel, T.N., 1986. Functional architecture of cortex revealed by optical imaging of intrinsic signals. *Nature* 324 (6095), 361–364.
- Grinvald, A., Lieke, E.E., Frostig, R.D., Hildesheim, R., 1994. Cortical point-spread function and long-range lateral interactions revealed by real-time optical imaging of macaque monkey primary visual cortex. *J. Neurosci.* 14 (5 Pt. 1), 2545–2568.
- Grinvald, A., Slovlin, H., Vanzetta, I., 2000. Non-invasive visualization of cortical columns by fMRI. *Nat. Neurosci.* 3 (2), 105–107.
- Gurden, H., Uchida, N., Mainen, Z., 2003. Presynaptic origin of odor-evoked intrinsic signal in olfactory glomeruli. *Abstr. - Soc. Neurosci.* 33, 489.5.
- Harel, N., Lee, S.P., Nagaoka, T., Kim, D.S., Kim, S.G., 2002a. Origin of negative blood oxygenation level-dependent fMRI signals. *J. Cereb. Blood Flow Metab.* 22 (8), 908–917.
- Harel, N., Zhao, F., Wang, P., Kim, S.-G., 2002b. Layer Specificity of BOLD and CBV fMRI Signals At Ultra-High Resolution. 8th International Conference on Functional Mapping of the Human Brain.
- Hayashi, T., Park, S.-H., Kim, S.-G., 2005. Relationship between intracortical vascular architecture and functional activation foci in high-resolution BOLD fMRI. 11th International Conference on Functional Mapping of the Human Brain.
- Hennig, J., Ernst, T., Speck, O., Deuschl, G., Feifel, E., 1994. Detection of brain activation using oxygenation sensitive functional spectroscopy. *Magn. Reson. Med.* 31 (1), 85–90.
- Hess, A., Stiller, D., Kaulisch, T., Heil, P., Scheich, H., 2000. New insights into the hemodynamic blood oxygenation level-dependent response through combination of functional magnetic resonance imaging and optical recording in gerbil barrel cortex. *J. Neurosci.* 20 (9), 3328–3338.
- Holthoff, K., Witte, O.W., 1996. Intrinsic optical signals in rat neocortical slices measured with near-infrared dark-field microscopy reveal changes in extracellular space. *J. Neurosci.* 16 (8), 2740–2749.
- Hu, X., Le, T.H., Ugurbil, K., 1997. Evaluation of the early response in fMRI in individual subjects using short stimulus duration. *Magn. Reson. Med.* 37 (6), 877–884.
- Hudetz, A.G., 1997. Blood flow in the cerebral capillary network: a review emphasizing observations with intravital microscopy. *Microcirculation* 4 (2), 233–252.
- Iadecola, C., Niwa, K., 2002. Nitric oxide. In: Edvinsson, L., Krause, D.N. (Eds.), *Cerebral Blood Flow and Metabolism*, 2nd ed. Lippincott Williams and Wilkins, Philadelphia, pp. 295–310.
- Iadecola, C., Yang, G., Ebner, T.J., Chen, G., 1997. Local and propagated vascular responses evoked by focal synaptic activity in cerebellar cortex. *J. Neurophysiol.* 78 (2), 651–659.
- Ishikawa, T., McDowall, D.G., 1980. Electrical activity of the cerebral cortex during induced hypotension with sodium nitroprusside and trimetaphan in the cat. *Br. J. Anaesth.* 53 (6), 605–611.
- Issa, N.P., Trepel, C., Stryker, M.P., 2000. Spatial frequency maps in cat visual cortex. *J. Neurosci.* 20 (22), 8504–8514.
- Jezzard, P., Rauschecker, J.P., Malonek, D., 1997. An in vivo model for functional MRI in cat visual cortex. *Magn. Reson. Med.* 38 (5), 699–705.
- Kalatsky, V.A., Stryker, M.P., 2003. New paradigm for optical imaging: temporally encoded maps of intrinsic signal. *Neuron* 38 (4), 529–545.
- Kennan, R.P., Scanley, B.E., Innis, R.B., Gore, J.C., 1998. Physiological basis for BOLD MR signal changes due to neuronal stimulation: separation of blood volume and magnetic susceptibility effects. *Magn. Reson. Med.* 40 (6), 840–846.
- Kim, S.G., 1995. Quantification of relative cerebral blood flow change by flow-sensitive alternating inversion recovery (FAIR) technique: application to functional mapping. *Magn. Reson. Med.* 34 (3), 293–301.
- Kim, D.S., Duong, T.Q., Kim, S.G., 2000a. High-resolution mapping of iso-orientation columns by fMRI. *Nat. Neurosci.* 3 (2), 164–169.
- Kim, D.S., Duong, T.Q., Kim, S.G., 2000b. Reply to “Can current fMRI techniques reveal the micro-architecture of cortex?” *Nat. Neurosci.* 3 (5), 414.
- Kinoshita, M., Gilbert, C.D., Das, A., 2003. Optical imaging of contextual interactions in V1 of the behaving monkey. *Abstr. - Soc. Neurosci.* 33, 484.5.
- Kontos, H.A., Wei, E.P., Navari, R.M., Levasseur, J.E., Rosenblum, W.I., Patterson Jr., J.L., 1978. Responses of cerebral arteries and arterioles to acute hypotension and hypertension. *Am. J. Physiol.* 234 (4), H371–H383.
- Kottenberg-Assenmacher, E., Armbruster, W., Bornfeld, N., Peters, J., 2003. Hypothermia does not alter somatosensory evoked potential amplitude and global cerebral oxygen extraction during marked sodium nitroprusside-induced arterial hypotension. *Anesthesiology* 98 (5), 1112–1118.
- Kwong, K.K., Belliveau, J.W., Chesler, D.A., Goldberg, I.E., Weisskoff, R.M., Poncelet, B.P., Kennedy, D.N., Hoppel, B.E., Cohen, M.S., Turner, R., et al., 1992. Dynamic magnetic resonance imaging of human brain activity during primary sensory stimulation. *Proc. Natl. Acad. Sci. U. S. A.* 89 (12), 5675–5679.
- Lindauer, U., Royl, G., Leithner, C., Kuhl, M., Gold, L., Gethmann, J., Kohl-Bareis, M., Villringer, A., Dirnagl, U., 2001. No evidence for early decrease in blood oxygenation in rat whisker cortex in response to functional activation. *NeuroImage* 13 (6), 988–1001.
- Liu, G.B., Zhang, Y., Pettigrew, J.D., Xu, W.F., Li, C.Y., 2003. Spreading and synchronization of intrinsic signals in visual cortex of macaque monkey evoked by a localized visual stimulus. *Brain Res.* 985 (1), 13–20.
- Logothetis, N., 2000. Can current fMRI techniques reveal the micro-architecture of cortex? *Nat. Neurosci.* 3 (5), 413–414.
- Lowel, S., Freeman, B., Singer, W., 1987. Topographic organization of the orientation column system in large flat-mounts of the cat visual cortex: a 2-deoxyglucose study. *J. Comp. Neurol.* 255 (3), 401–415.
- Lu, H., Patel, S., Luo, F., Li, S.J., Hillard, C.J., Ward, B.D., Hyde, J.S., 2004. Spatial correlations of laminar BOLD and CBV responses to rat whisker stimulation with neuronal activity localized by Fos expression. *Magn. Reson. Med.* 52 (5), 1060–1068.
- MacVicar, B.A., Hochman, D., 1991. Imaging of synaptically evoked intrinsic optical signals in hippocampal slices. *J. Neurosci.* 11 (5), 1458–1469.
- Maekawa, T., McDowall, D.G., Okuda, Y., 1979. Brain-surface oxygen tension and cerebral cortical blood flow during hemorrhagic and drug-induced hypotension in the cat. *Anesthesiology* 51 (4), 313–320.
- Malonek, D., Grinvald, A., 1996. Interactions between electrical activity and cortical microcirculation revealed by imaging spectroscopy: implications for functional brain mapping. *Science* 272 (5261), 551–554.

- Mandeville, J.B., Marota, J.J., 1999. Vascular filters of functional MRI: spatial localization using BOLD and CBV contrast. *Magn. Reson. Med.* 42 (3), 591–598.
- Mandeville, J.B., Marota, J.J., Kosofsky, B.E., Keltner, J.R., Weissleder, R., Rosen, B.R., Weisskoff, R.M., 1998. Dynamic functional imaging of relative cerebral blood volume during rat forepaw stimulation. *Magn. Reson. Med.* 39 (4), 615–624.
- Mayhew, J.E., Askew, S., Zheng, Y., Porrill, J., Westby, G.W., Redgrave, P., Rector, D.M., Harper, R.M., 1996. Cerebral vasomotion: a 0.1-Hz oscillation in reflected light imaging of neural activity. *NeuroImage* 4 (3 Pt. 1), 183–193.
- McDowall, D.G., Keane, N.P., Turner, J.M., Lane, J.R., Okuda, Y., 1974. The toxicity of sodium nitroprusside. *Br. J. Anaesth.* 46 (5), 327–332.
- McHedlishvili, G., Kuridze, N., 1984. The modular organization of the pial arterial system in phylogeny. *J. Cereb. Blood Flow Metab.* 4 (3), 391–396.
- Menon, R.S., Goodyear, B.G., 1999. Submillimeter functional localization in human striate cortex using BOLD contrast at 4 Tesla: implications for the vascular point-spread function. *Magn. Reson. Med.* 41 (2), 230–235.
- Menon, R.S., Ogawa, S., Hu, X., Strupp, J.P., Anderson, P., Ugurbil, K., 1995. BOLD based functional MRI at 4 Tesla includes a capillary bed contribution: echo-planar imaging correlates with previous optical imaging using intrinsic signals. *Magn. Reson. Med.* 33 (3), 453–459.
- Menon, R.S., Ogawa, S., Strupp, J.P., Ugurbil, K., 1997. Ocular dominance in human V1 demonstrated by functional magnetic resonance imaging. *J. Neurophysiol.* 77 (5), 2780–2787.
- Michenfelder, J.D., Milde, J.H., 1988. The interaction of sodium nitroprusside, hypotension, and isoflurane in determining cerebral vasculature effects. *Anesthesiology* 69 (6), 870–875.
- Morris, P.J., Heuser, D., McDowall, D.G., Hashiba, M., Myers, D., 1983. Cerebral cortical extracellular fluid H⁺ and K⁺ activities during hypotension in cats. *Anesthesiology* 59 (1), 10–18.
- Nagaoka, T., Harel, N., Zhao, F., Wang, P., Kim, S.G., 2002. Critical threshold of arterial blood pressure for BOLD responses to visual stimulation in anesthetized cats. *Proc. Int. Soc. Mag. Reson.*, 10.
- Nagaoka, T., Zhao, F., Wang, P., Harel, N., Kennan, R.P., Ogawa, S., Kim, S.G., in press. Increases in oxygen consumption without cerebral blood volume change during visual stimulation under hypotension condition. *J. Cereb. Blood Flow Metab.*
- Narayan, S.M., Santori, E.M., Blood, A.J., Burton, J.S., Toga, A.W., 1994. Imaging optical reflectance in rodent barrel and forelimb sensory cortex. *NeuroImage* 1 (3), 181–190.
- Narayan, S.M., Esfahani, P., Blood, A.J., Sikkens, L., Toga, A.W., 1995. Functional increases in cerebral blood volume over somatosensory cortex. *J. Cereb. Blood Flow Metab.* 15 (5), 754–765.
- Nomura, Y., Fujii, F., Sato, C., Nemoto, M., Tamura, M., 2000. Exchange transfusion with fluorocarbon for studying synaptically evoked optical signal in rat cortex. *Brain Res. Brain Res. Protoc.* 5 (1), 10–15.
- Offenhauser, N., Thomsen, K., Caesar, K., Lauritzen, M., 2005. Activity-induced tissue oxygenation changes in rat cerebellar cortex: interplay of postsynaptic activation and blood flow. *J. Physiol.* 565 (Pt. 1), 279–294.
- Ogawa, S., Lee, T.M., Kay, A.R., Tank, D.W., 1990. Brain magnetic resonance imaging with contrast dependent on blood oxygenation. *Proc. Natl. Acad. Sci. U. S. A.* 87 (24), 9868–9872.
- Orbach, H.S., Cohen, L.B., 1983. Optical monitoring of activity from many areas of the in vitro and in vivo salamander olfactory bulb: a new method for studying functional organization in the vertebrate central nervous system. *J. Neurosci.* 3 (11), 2251–2262.
- Park, S.-H., Hayashi, T., Kim, S.-G., 2005. Determination of intracortical venous vessel density using venography at 9.4 T. *Proc. Int. Soc. Magn. Reson.*, 13.
- Pinaud, M., Souron, R., Lelassque, J.N., Gazeau, M.F., Lajat, Y., Dixneuf, B., 1989. Cerebral blood flow and cerebral oxygen consumption during nitroprusside-induced hypotension to less than 50 mmHg. *Anesthesiology* 70 (2), 255–260.
- Rao, S.C., Toth, L.J., Sur, M., 1997. Optically imaged maps of orientation preference in primary visual cortex of cats and ferrets. *J. Comp. Neurol.* 387 (3), 358–370.
- Ratzlaff, E.H., Grinvald, A., 1991. A tandem-lens epifluorescence microscope: hundred-fold brightness advantage for wide-field imaging. *J. Neurosci. Methods* 36 (2–3), 127–137.
- Rovainen, C.M., Woolsey, T.A., Blocher, N.C., Wang, D.B., Robinson, O.F., 1993. Blood flow in single surface arterioles and venules on the mouse somatosensory cortex measured with videomicroscopy, fluorescent dextrans, nonoccluding fluorescent beads, and computer-assisted image analysis. *J. Cereb. Blood Flow Metab.* 13 (3), 359–371.
- Sato, M., Pawlik, G., Umbach, C., Heiss, W.D., 1984. Comparative studies of regional CNS blood flow and evoked potentials in the cat. Effects of hypotensive ischemia on somatosensory evoked potentials in cerebral cortex and spinal cord. *Stroke* 15 (1), 97–101.
- Schumann, P., Touzani, O., Young, A.R., Morello, R., Baron, J.C., MacKenzie, E.T., 1998. Evaluation of the ratio of cerebral blood flow to cerebral blood volume as an index of local cerebral perfusion pressure. *Brain* 121 (Pt. 7), 1369–1379.
- Schumann-Bard, P., Touzani, O., Young, A.R., Toutain, J., Baron, J.C., Mackenzie, E.T., Schmidt, E.A., 2005. Cerebrovascular effects of sodium nitroprusside in the anesthetized baboon: a positron emission tomographic study. *J. Cereb. Blood Flow Metab.* 25 (4), 535–544.
- Sharon, D., Grinvald, A., 2002. Dynamics and constancy in cortical spatiotemporal patterns of orientation processing. *Science* 295 (5554), 512–515.
- Sheth, S.A., Nemoto, M., Guiou, M., Walker, M., Pouratian, N., Hageman, N., Toga, A.W., Sheth, S., 2004. Columnar specificity of microvascular oxygenation and volume responses: implications for functional brain mapping. *J. Neurosci.* 24 (3), 634–641.
- Shmuel, A., Grinvald, A., 1996. Functional organization for direction of motion and its relationship to orientation maps in cat area 18. *J. Neurosci.* 16 (21), 6945–6964.
- Silva, A.C., Lee, S.P., Iadecola, C., Kim, S.G., 2000. Early temporal characteristics of cerebral blood flow and deoxyhemoglobin changes during somatosensory stimulation. *J. Cereb. Blood Flow Metab.* 20 (1), 201–206.
- Takashima, I., Kajiwara, R., Iijima, T., 2001. Voltage-sensitive dye versus intrinsic signal optical imaging: comparison of optically determined functional maps from rat barrel cortex. *NeuroReport* 12 (13), 2889–2894.
- Thompson, J.K., Peterson, M.R., Freeman, R.D., 2003. Single-neuron activity and tissue oxygenation in the cerebral cortex. *Science* 299 (5609), 1070–1072.
- Tomita, M., Gotoh, F., Yamamoto, M., Tanahashi, N., Kobari, M., 1983. Effects of hemolysis, hematocrit, RBC swelling, and flow rate on light scattering by blood in a 0.26 cm ID transparent tube. *Biorheology* 20 (5), 485–494.
- Toth, L.J., Rao, S.C., Kim, D.S., Somers, D., Sur, M., 1996. Subthreshold facilitation and suppression in primary visual cortex revealed by intrinsic signal imaging. *Proc. Natl. Acad. Sci. U. S. A.* 93 (18), 9869–9874.
- Tusa, R.J., Rosenquist, A.C., Palmer, L.A., 1979. Retinotopic organization of areas 18 and 19 in the cat. *J. Comp. Neurol.* 185 (4), 657–678.
- van Bruggen, N., Busch, E., Palmer, J.T., Williams, S.P., de Crespigny, A.J., 1998. High-resolution functional magnetic resonance imaging of the rat brain: mapping changes in cerebral blood volume using iron oxide contrast media. *J. Cereb. Blood Flow Metab.* 18 (11), 1178–1183.
- Vanzetta, I., Grinvald, A., 1999. Increased cortical oxidative metabolism due to sensory stimulation: implications for functional brain imaging. *Science* 286 (5444), 1555–1558.

- Vanzetta, I., Slovin, H., Omer, D.B., Grinvald, A., 2004. Columnar resolution of blood volume and oximetry functional maps in the behaving monkey; implications for fMRI. *Neuron* 42 (5), 843–854.
- Woolsey, T.A., Rovainen, C.M., Cox, S.B., Henegar, M.H., Liang, G.E., Liu, D., Moskalenko, Y.E., Sui, J., Wei, L., 1996. Neuronal units linked to microvascular modules in cerebral cortex: response elements for imaging the brain. *Cereb. Cortex* 6 (5), 647–660.
- Zhao, F., Wang, P., Kim, S.G., 2004a. Cortical depth-dependent gradient-echo and spin-echo BOLD fMRI at 9.4 T. *Magn. Reson. Med.* 51 (3), 518–524.
- Zhao, F., Wang, P., Ugurbil, K., Kim, S.G., 2004b. Cortical layer-dependent basal CBV and stimulation-induced CBV responses. *Proc. Int. Soc. Mag. Reson.*, 12.
- Zhao, F., Wang, P., Hendrich, K., Kim, S.-G., 2005. Spatial specificity of cerebral blood volume-weighted fMRI responses at columnar resolution. *NeuroImage* 27 (2), 416–424.